Quantitative SPECT Imaging: A Review and Recommendations by the Focus Committee of the Society of Nuclear Medicine Computer and Instrumentation Council

M.S. Rosenthal, J. Cullom, W. Hawkins, S.C. Moore, B.M.W. Tsui and M. Yester

Department of Diagnostic Radiology, University of Pittsburgh, Pittsburgh, Pennsylvania; Department of Radiology, Emory University, Atlanta, Georgia; Department of Radiology, University of Nebraska Medical Center, Omaha, Nebraska; Nuclear Medicine Service, Harvard Medical School and Department of Veterans Affairs Medical Center, W. Roxbury, Massachusetts; Department of Radiology and Biomedical Engineering, University of North Carolina, Chapel Hill, North Carolina, and Division of Nuclear Medicine, University of Alabama, Birmingham, Alabama

This article is a review of the physics principles, instrumentation and reconstruction methods behind SPECT imaging. Particular attention is paid to the mechanisms that can significantly affect the accuracy of a SPECT image. We describe instrumentation advances and reconstruction methods used to correct images to improve image quality and produce quantitative images. The clinical importance of improved image quality and quantitation are also reviewed.

Key Words: single-photon emission computed tomography; quantitation; image quality

J Nucl Med 1995; 36:1489–1513

The increasing interest in quantitative imaging and improved image quality in SPECT motivated the Computer and Instrumentation Council (CIC) to investigate state-of-the-art of quantitative imaging and produce a report detailing the different factors affecting quantitation and providing recommendations for SPECT practitioners.

This article presents the physics background relevant to quantitative imaging, advantages and disadvantages of quantitative imaging, a discussion on what areas of SPECT imaging can benefit from improved imaging, as well as examples of implementation. We will not, however, cover other important topics in quantitative imaging such as PET, time-activity curve generation or physiological modeling.

Obvious questions that can be posed by clinicians are: Why should one strive to accomplish quantitative imaging and what advantages does it provide to the general nuclear medicine clinician and research investigator? A major benefit of quantitative imaging will be improved quantitative accuracy, image quality and/or diagnostic ability. After correcting for attenuation and scatter, the resultant images will represent the activity distribution of the injected tracer more accurately. The implementation of quantitative imaging procedures therefore would improve important image characteristics, such as contrast, signal-to-noise ratios and, potentially, resolution. One drawback may be the increased noise for the same number of raw counts detected. In general, resultant images will provide a more accurate representation of the tissue activity after corrections.

There are many potential benefits of quantitative imaging. For example, a typical application of quantitative imaging techniques would be monoclonal antibody imaging for either diagnosis or treatment. To determine the necessary dose of monoclonal antibodies for treatment of a disease, the target-to-injection ratio and the tissue-specific activity are needed. This is not possible with current SPECT techniques, but it would be possible to measure both of these quantities with quantitative SPECT.

Another procedure which could benefit from quantitative imaging is the myocardial perfusion stress/redistribution study. Currently, physicians look at the patients' images and plots of activity as a function of circumferential distance around the myocardium. They also estimate the ratios of the stress-to-redistribution activities and compare these curves to a normal database. The same gamma camera used for both stress and redistribution studies are important in this type of study. The use of quantitative imaging techniques would aid thallium stress studies in several ways. For example, the physician would be relieved from using the same gamma camera for both parts of the study because the images would provide estimates of true tissue-

Received May 11, 1994; revision accepted Jan. 3, 1995.

For correspondence contact: Marc S. Rosenthal, PhD, Department of Surgery, University of Pittsburgh, Center for Biotechnology and Bioengineering, 300 Technology Dr., Pittsburgh, PA 15219.

specific activity directly. The physician would not only be able to report the activity curves and ratios, but could also compare these absolute curves with the injected dose to estimate organ uptake. This might be especially useful in patients with uniform three-vessel disease.

Additionally, quantitative imaging techniques might provide improved image quality and lesion detectability. A major handicap for the nuclear medicine reader is background noise in images in conjunction with poor target-to-background ratios, i.e., poor contrast. The use of quantitative techniques could improve the visualized lesion contrast resulting in improved image quality and spatial resolution at a minimum and, depending on the noise properties, perhaps a concomitant increase in lesion detectability.

The following definitions will be helpful in review of this article.

Relative Quantitation

Comparison of counts between two different sets of data irrespective of means or methods of data acquisition. Examples of relative quantitation include the comparison of counts within two different regions of interest (ROI) within the same image, or from two or more different images. It can also be the comparison of counts/intensities between abnormal and normal databases.

Absolute Quantitation

The determination of the actual tissue activity (e.g., mCi/100 g). This implies the accurate application of corrections to the data to determine the activity within a defined region. This absolute determination can be made for an area or a volume. In addition, the absolute quantitation can determine either the concentration of radioactivity or the total activity in the defined region. The activity can also be compared to the injected dose. Results can be compared from case to case without regard to imaging methods or size of patient.

Precision

Precision is a measure of how a result is determined without reference or knowledge to any true value (*1*). For example, if a measurement is reported to be 2.002 m (2.002 ± 0.001), then the absolute precision of this measurement is on the order of 1 mm, whereas the relative precision is 1/2000. Any correction for systematic errors may improve the accuracy of the measurement but not the precision. Essentially, the precision of a measurement will be dependent upon the control and analysis of random errors.

Accuracy

Accuracy of a measurement is a measure of how close the results are to the truth (*1*). The accuracy of a measurement will be dependent on the control and correction of systematic errors. A measurement of 2.002 m is more accurate than 2.0 m. In the first case, the accuracy is to a millimeter, while in the second case the accuracy is to 10 cm.

Quantified and Quantitate

To quantitate a measurement indicates that the measurement is to be made as precise and as accurate as possible with the goal of producing an absolute measurement.

Attenuation

The class of photons which is most useful for SPECT imaging consists of those photons that originate from a nuclear decay, follow a straight-line trajectory through a collimator hole, and deposit their full energy in the NaI(Tl) crystal. Attenuation is the loss of these useful photons, either by photoelectric absorption or by scatter through an angle sufficiently large that they can no longer be detected. When a collimated beam of photons of intensity, I_O, passes through a thickness, x, of a given material, the intensity exiting the material (as determined with a very small, collimated detector) is given by:

$$I = I_O e^{-\mu x}, \qquad \text{Eq. 1}$$

where μ is the linear attenuation coefficient, which fundamentally depends upon the material composition and photon energy. In addition, μ depends upon the experimental geometry used to make the measurement. Using narrow-beam geometry, in which the beam incident on the material is highly collimated, a true measurement of μ may be obtained (The true value, however, is only approached asymptomatically as the beam is made narrower). If the measurement is instead made with a broad beam, photons from regions other than that of the beam may be scattered into the detector, thereby increasing the detected intensity above what would otherwise be expected. In this case, the value of μ calculated from the experiment is smaller than when obtained using a narrow beam. In nuclear medicine imaging the photons traverse the patient in all directions, which is characteristic of a very broad-beam geometry. The narrow-beam attenuation coefficient for 140-keV photons in water is 0.15 cm^{-1}, while the broad-beam coefficient appropriate for most imaging geometries (thoracic or abdominal imaging) is approximately 0.12 cm^{-1} (*2*).

Scatter

Photons which scatter in the patient that are not detected are considered to have been attenuated by the patient. Because of broad-beam geometry and finite energy resolution many scattered photons are in fact detected. If a photon undergoes a coherent scatter before detection (which changes its direction but not its energy), the photon will be indistinguishable from a good photon (a primary, unscattered photon). Even Compton scattered photons, which are far more abundant at nuclear medicine energies than coherently scattered photons, often cannot be separated from primary photons. For example, a single small-angle Compton scatter only decreases the photon energy minimally. A 140-keV photon scattered through an angle of 52° produces a photon with 126 keV which is within a 20% energy window. Since the photon energies can only be measured by the detector with a precision of about 10%–12% (for ^{99m}Tc), a wide (15%–20%) pulse-height discrimi-

nator window is usually chosen to include most of the unscattered photons. The imperfect determination of energy by the detector means that many Compton scattered photons can still be recorded in the photopeak window of the camera's pulse-height analyzer.

Energy Resolution

Energy resolution refers to the precision with which the detector can determine the energy of a detected photon. It is usually reported as the FWHM of the photopeak divided by the photopeak energy (×100%). The imperfect measurement of energy results primarily from the statistical uncertainty in the number of light photons and, ultimately, photomultiplier tube (PMT) electrons produced by each primary photon (e.g., gamma ray photon) interaction in the NaI(Tl) crystal. In comparing two cameras of different energy resolution, the camera with the better energy resolution can better separate Compton scattered from primary photons.

Detector Response and System Spatial Resolution

The detector response describes how the imaging system blurs the image of a point-source of radiation spatially. For this reason, the spatial resolution of the imaging system is often described by a function called the point-spread function (PSF) of the imaging system. The PSF includes the combined effects of scatter, collimator and detector blur on the image. The Fourier transform of the PSF is called the modulation transfer function (MTF) of the imaging system. There are two contributions to the detector PSF which can be mathematically described as the convolution of: (a) the Anger camera's intrinsic PSF with (b) the collimator PSF. The FWHM of the collimator PSF increases approximately linearly with increasing distance from the collimator surface (i.e., the spatial resolution worsens with increasing distance between the source and the camera). When the spatial resolution is not the same for all source locations, the PSF is said to be nonstationary. If a SPECT study is performed, a point source which is imaged close to the camera at one point in the camera's rotation will be farther away, for example, when the opposing projection is acquired. This means that the reconstructed three-dimensional response function will be a weighted average PSF. Thus, the SPECT reconstruction from 360° projection data can reduce the distance dependence of the detector response. This type of reconstruction algorithm can also influence the degree to which the three-dimensional PSF can be made more stationary. Additionally, if the reconstructed resolution can be made the same in all directions, the PSF is said to be isotropic.

In addition to the detector response, the overall system spatial resolution includes effects introduced by the reconstruction algorithm. For example, if a smooth reconstruction filter is used, the system spatial resolution would be worse than that obtained using a ramp filter alone. It should be emphasized that the conventional filtered backprojection reconstruction does produce an asymmetric PSF because this linear algorithm does not correct for the distance-dependent detector response.

Contrast

Contrast of the image of a feature (e.g., lesion) embedded in a uniform background is defined as the difference between the average image brightness (or pixel value) inside the feature and the average brightness in the background, divided by the background brightness. Thus, if the background contains 100 counts/pixel and the lesion contains 120 counts/pixel, the contrast would be (120–100)/100 = 0.2, or 20% (in some definitions, the difference is divided by the average of the lesion-to-background values. In an image of a lesion which is small compared to the spatial resolution (FWHM of the PSF), the peak contrast measured at the center of the lesion can be reduced significantly because of blurring by the detector response. In fact, even for structures which are large compared to the geometric spatial resolution, the long tails on the PSF contributed by scattered photons also degrade contrast significantly.

Noise, Noise Correlations and Noise Power Spectrum

Image noise is the degree of variability of the pixel values caused by the statistical nature of the radioactive decay and detection processes. If many identical planar projection images of a large, uniform radioactivity distribution are acquired, each for the same scan time, the properties of poisson counting statistics allow us to make several predictions about the characteristics of the image noise. First, the statistical fluctuations observed in any one image pixel will be entirely independent of the fluctuations in the other pixels. In this case, the image noise is spatially uncorrelated. Second, if the average value of the counts in a given pixel (over the whole set of images) is equal to N, then the standard deviation of the counts in the same pixel over the set of images is expected to be $N^{1/2}$. Third, if we calculate the standard deviation over many pixels in a uniform region of a single image instead, we would also expect to obtain $N^{1/2}$ for this case.

When a tomographic image is reconstructed, the image noise properties change significantly. The reconstruction process causes the pixel noise in a tomographic slice to be positively correlated at short distances and negatively correlated at longer distances. This means that if a given pixel's value is greater than its expected value, then the pixels located (in the same transaxial image) around this pixel at a given radius will have pixel values that are greater than or less than their expected values. This also implies that a standard deviation calculated from the pixels inside a uniform ROI on a single transaxial SPECT slice will not simply be equal to the square root of the average pixel value, but rather, will depend upon the size and shape of the ROI. In addition, because the noise in SPECT projections is nonstationary (since the projection values fall off to zero near the edges of the field of view (FOV)), the reconstructed pixel noise will also be nonstationary. These comments are particularly true when using a ramp filter.

The noise power spectrum (NPS), which is a measure of

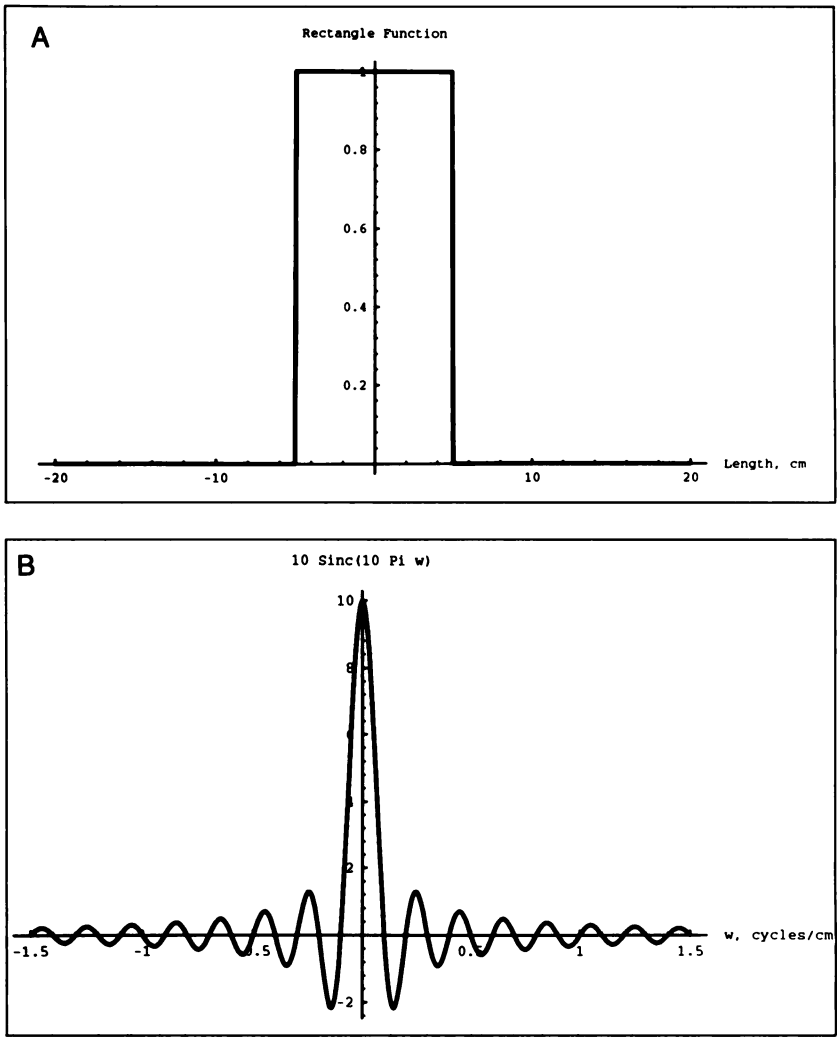

FIGURE 1. (A) A rectangle function of width 10 cm. The rectangle function is the quintessential band limited function. (B) The Fourier transform of the rectangle function of Figure 1A.

the magnitude of the noise as a function of frequency, of uncorrelated noise is constant; this means that this type of image noise is the same at all spatial frequencies (also called white noise). By contrast, the NPS of spatially correlated noise is said to be colored because the frequency spectrum is not constant. By using a smoother filter when reconstructing tomographic images, the image noise changes in two ways: (a) the total noise variance is reduced and (b) the correlation length is increased, thereby creating the appearance of larger noise blobs in the image.

Linear systems

SPECT imaging processes should and can be made linear. A measuring device is linear if the action of the device upon the sum of two elements of input is the same as the action upon each element separately, and then adding the outputs together. A volt meter or galvanometer is an example of a linear measurement. Measuring two voltage sources separately and summing the voltages is the same as performing one measurement with the two voltage sources in series.

Is the projection image provided by a SPECT system an example of a linear transformation? The answer is yes, provided that we can neglect thermal noise of the photomultipliers and background radiation in the regions of the image with low counts, and also that we keep the count rate low enough so that pulse pile up and camera resolving time are not significant. Thus, it is easy to see that if we have two sources, and we image them separately and then combine the images, this should be the same (up to noise) as imaging them both together.

Fourier Transforms and Bandwidth Functions

The importance of Fourier transform methods to SPECT reconstruction and image processing cannot be overstressed. The Fourier transform has many important and useful properties. The Fourier transform of a function f(x) is its expansion as a series of the trigonometric functions $\cos(\omega x)$ and $\sin(\omega x)$. The quantity ω is the angular (spatial) frequency. The units of ω are the reciprocal of the units of x. Thus, if x has units in centimeters, ω has units of 1/cm.

The term bandwidth refers to the domain x over which a function f(x) is nonzero. A function or physical quantity is bandlimited if it is nonzero only within a finite domain. For

SPECT projection data, this domain is the set of pixels that constitute the planar image.

A function f(x) and its Fourier transform cannot both be bandlimited. In fact, a bandlimited function will always possess a Fourier transform that is very smooth (defined) everywhere and is of infinite extent in its domain (*3*). In other words, the Fourier transform of a bandlimited function is not bandlimited.

When we apply Fourier transform methods to SPECT and medical image processing, we require that the Fourier transform be bandlimited. If we truncate a Fourier transform that is not bandlimited, a severe artifact known as ringing is generated in the final image. The amplitude and frequency of the ringing is highly dependent upon the amplitude and frequency of the first truncated frequency (*4*).

A generic example of a bandlimited function is a rectangle and its Fourier transform which, as promised, is continuous, nonzero almost everywhere and of infinite extent (Fig. 1).

One method to obtain a bandlimited Fourier transform is to use a low-pass filter. In this approach, a low-pass filter is designed so that it passes the low frequencies with little or no change, but reduces the magnitudes of or eliminates the higher frequencies. While this procedure diminishes the high frequencies that caused the ringing, it can have a serious side effect. The problem with this approach is that the noise becomes correlated in image space. That is, the noise from adjacent pixels is mixed together to form the noise in the image, yielding noise blobs of low-pass filtering. In addition, the use of low-pass filtering can worsen the reconstructed spatial resolution.

Partial Volume Effect

The partial volume effect for digital images refers to the mismatch between the system resolution, object size and pixel size. This mismatch can produce images which do not depict the object properly. For tomographic reconstruction, the system resolution is defined as the FWHM of the camera point response function, measured at all camera-source positions. First, let us assume that we have chosen a pixel size that matches the resolution of the camera. According to the sampling theorem, we should choose a pixel size that is at least one half the size of the FWHM of the system point response function (SPRF), assuming a Gaussian-shaped function. For collimator effects, the SPRF can be approximated by a Gaussian function. To illustrate the qualitative nature of the partial volume effect, we have shown the effect of the system point response function on a one-dimensional rectangular object 2 cm in length. We then blurred the object with Gaussian distributions with different FWHMs. The overall effect is to smear the binary object over a larger length (Fig. 2).

If we attempted to quantify the amount of activity by using a template (test image) of the original object, we would not recover all of the activity. As the length of the object becomes larger with respect to the FWHM of the imaging system, we recover a greater fraction of the activity.

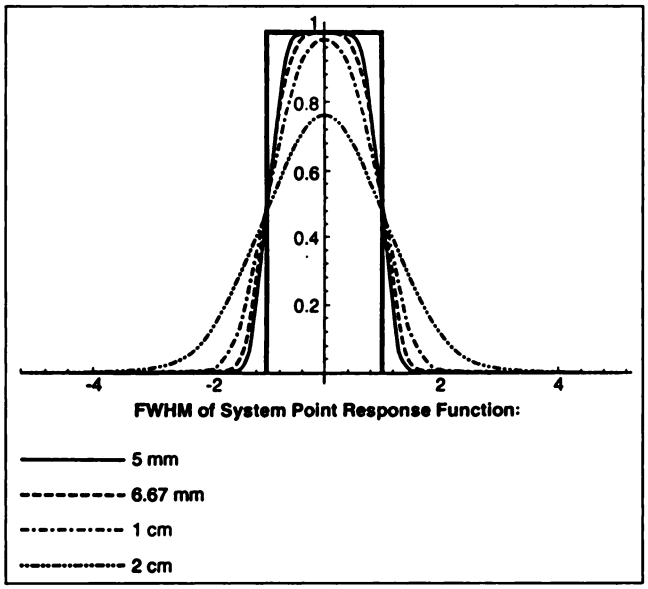

FIGURE 2. The system point response function (one-dimensional case). A rectangle convolved with the Gaussian function with FWHMs of 0.5, 0.6667, 1 and 2 cm.

It is not necessarily true that we recover more of the activity from a template as the FWHM of the imaging system becomes smaller with respect to the length of the object. We must consider the pixel size; if the pixel size also decreases so as to remain constant with respect to the FWHM, then the assertion is true.

A contemporary SPECT system can have quite good resolution, so matching the pixel size to the system resolution should not be overlooked. Undersampling or the use of a pixel dimension that is too large produces distortions described as aliasing. In general, for objects with large high frequency components (small, focal objects), aliasing will be more evident than in objects with small high frequency components (large, systemic objects). Hence, aliasing becomes important as we approach the resolution limit of the system.

The overall partial volume effect in SPECT is complicated because the tomographic, or reconstructed PRF is nonstationary, nonisotropic and non-Gaussian, depending on the type of reconstruction algorithm, attenuating medium and protocol. Basically, the partial volume effect, unless compensated for, will make quantification unreliable for objects smaller than about three to four times the system FWHM.

Ill-Posed Problems

No discussion of SPECT would be complete without an attempt to define the concept, ill-posed problems, that underlies many of the approaches to problems in medical tomography, imaging science and SPECT, in particular. Physicists and mathematicians use mathematical models of physical phenomena to study them to predict the behavior and infer new facts. All such models are initialized in time

by initial conditions, or spatially constrained by boundary conditions. In the real world, these initializing or constraining data are obtained by physical measurements that are not necessarily accurate or precise (i.e., they may be degraded by noise or systematic errors). If the model produces a correspondingly small error for some small error in the data, then the model is said to be well-posed. Conversely, if the model produces an error which cannot be simply predicted from a small data error, than this model is ill-posed.

The degree to which a problem is ill-posed has a great influence upon how readily we can find the solution. Reconstruction in the presence of noise becomes increasingly ill-posed as the noise level rises. Therefore, a reconstruction algorithm must be more robust or well-posed as the noise level of the data increases so as to produce results which are accurate.

FACTORS AFFECTING QUANTITATION

Overall ability to perform accurate quantitation depends on the quantity and quality of the data that forms the image. The quantity of photons depends on factors related to the patient, physical factors (attenuation and scatter), technical factors related to the instrumentation, and procedural factors (acquisition specific). The quality of the image (fidelity to the original object) will depend on physical (scatter), technical (imaging characteristics), and procedural factors. Once the raw data have been obtained in a SPECT acquisition then the final image will depend on the processing, reconstruction and compensation methods (which can affect quality and quantitative accuracy). Finally, the ultimate quantitation of structures within the image will be obtained from some processing. These factors will be considered in some detail in the following.

Patient Limitations

Final images represent the convolution of the gamma camera spatial resolution, scatter and attenuation with the object such that the image is degraded relative to the original object. In the case being discussed here, the object is the patient or a particular structure within the patient. A primary factor in quantitation and imaging is the amount of information available, that is, counting or imaging statistics. The number of photons emitted per unit of time available for detection depends on the fraction of the administered dose in a specific organ at the time of imaging and the amount of attenuation the photons experience before reaching the detector. Thus, imaging statistics are a function of the administered dose, biokinetics involved and patient size.

The image contrast produced in nuclear medicine studies is dependent upon the spatial distribution of activity within the area of interest. The spatial distribution and its changes in time (biokinetics) are dependent upon the rate of tracer uptake (input function), the tissue extraction of the tracer and finally the trapping or metabolism of the administered tracer. Following metabolism or trapping of the tracer as blood concentration decreases, the tracer will generally wash out of the cell compartment. The uptake, metabolism and excretion of the tracer, in conjunction with the tracer's physical half-life, will define an effective decay rate and half-life. Under optimal conditions, the total statistics generated in a study will then be a function of the time integral of the spatially varying activity during image acquisition. The biokinetics of the tracer along with other factors will limit the total available statistics for the study.

The administered dose is generally limited by the critical organ radiation dose. Not uncommonly, this organ is not of primary interest but because of the distribution of the administered radiopharmaceutical it limits the administered dose.

Since image quality in nuclear medicine is limited by statistics, the imaging time is extremely important, and is most often dictated by the tolerance of the patient to the procedure. If the tolerance is exceeded, patient motion relative to the imaging device, will often result and thus affect the results through the entire imaging sequence. The effect of patient motion is quite complex, as it depends on the magnitude and duration of motion. Analyses of motion on ^{201}Tl SPECT have been provided by Prigent et al. (*5*), Cooper et al. (*6*) and Botvinick et al. (*7*).

Finally, the patient habitus will affect the amount of attenuation (fraction of emitted photons that exit the body) and the amount of scattered photons (degradation) that are detected. For example, with narrow beam geometry, one-half of the available photons are attenuated in 3.6 cm of soft tissue at 70 keV, 4.5 cm at 140 keV; and 6.2 cm at 364 keV.

Technical Factors

It should be stressed that the imaging hardware fundamentally limits the information available for any given quantitative procedure. If SPECT projection data are acquired with an inappropriate collimator, for example, the resulting quantitative accuracy (or precision) may be significantly degraded. Although post-processing (e.g., restoration filtering) may improve the quantitation somewhat, one cannot generally obtain results that are equivalent to those obtained under optimal conditions of data acquisition.

Choice of Collimator. It is well known that the collimator design primarily determines the tradeoff between spatial resolution and detection efficiency, both of which can affect quantitation significantly. Spatial resolution can limit the contrast of any lesion to be quantified, thereby influencing the accuracy of activity or size quantitation. The image counts determine the noise level in the image and thus the precision with which quantitation may be accomplished.

Parallel Collimation. The geometric spatial resolution, efficiency and penetration fraction of a parallel, multi-hole camera collimator were first discussed by Anger (*8*). The geometric parameters of such a collimator are depicted in Figure 3, along with three types of events which should be considered. The desirable, geometrically collimated pho-

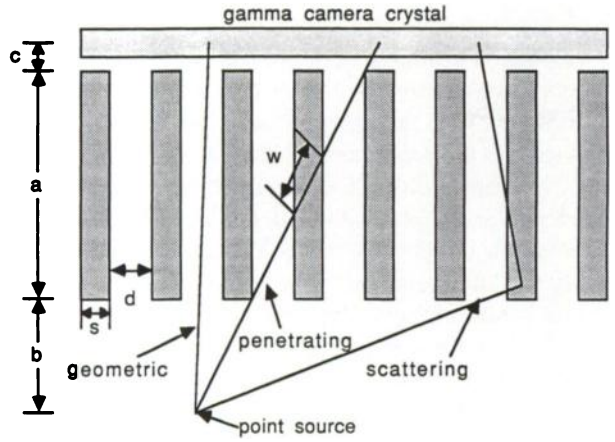

FIGURE 3. Collimator geometric parameters and types of photon interactions (reprinted with permission from Moore et al. (*129*).

tons (i.e., gamma rays) traverse the collimator entirely within a single hole, without striking any septal material. Penetrating gammas go through one or more septal walls without interacting, while scattered photons are deflected into the Anger camera by a Compton or coherent interaction in a septum. The collimator penetration and scatter components are generally undesirable because their point of origin in the source does not correspond directly with their point of detection in the scintillation camera. Large numbers of penetrating or scattering photons can contribute a substantial background to the image, thereby degrading the contrast of important image features.

The spatial resolution of a parallel-hole collimator, expressed as the FWHM of the point spread function (PSF), is approximately:

$$r_c = d(a + b + c)/a_e, \qquad \text{Eq. 2}$$

where d is the collimator hole size (Fig. 3), a is the collimator thickness, a_e is the effective collimator thickness ($a_e = a - 2/\mu$), where μ is the total linear attenuation coefficient of the collimator material at the relevant energy), b is the source-to-collimator distance and c is the mean interaction depth in the detector. This equation was modified from Anger (*8*) by considering that the collimator hole length, a, should be reduced on both ends by approximately $1/\mu$ due to penetration effects (*9,10*). Of course, the single parameter, r_c in Equation 2 does not offer a complete description of the collimator's PSF or its Fourier transform, the MTF, whose detailed shapes depend upon the shape of the collimator holes. Nevertheless, for the same hole area the exact shape of the collimator holes has only a small influence on the radially averaged MTF of a parallel-hole collimator as compared to the choice of other geometric parameters, such as hole size, hole length and source distance (*11,12*).

It is clear from Equation 2 that the spatial resolution of the collimator worsens linearly with increasing distance from the collimator face. Also, it should be noted that the resolution changes less over a given range of collimator-source distances, b, for larger values of collimator thickness, a. In other words, the slope of the resolution versus distance line is less for thicker collimators. Under these conditions, therefore, we would expect a more stationary PSF over the tomographic FOV.

The overall system resolution of a gamma camera image is given by the convolution of the collimator PSF with the intrinsic camera PSF. The intrinsic PSF is usually well approximated by a radially symmetric Gaussian function, with an ~3–4 mm FWHM for a modern scintilliation camera. For the sake of simplicity, if we also approximate the collimator's PSF by a Gaussian, then the approximate combined system spatial resolution FWHM is given by the quadrature sum:

$$r_s = (r_c^2 + r_i^2)^{1/2}. \qquad \text{Eq. 3}$$

The collimator's geometric efficiency is simply the fraction of isotropically emitted gamma photons from a point source that enter the collimator properly. This efficiency is effectively independent of source-collimator distance (under usual imaging conditions) and is given by:

$$g = (kd^2/[a_e(d + s)])^2, \qquad \text{Eq. 4}$$

where k is a factor which depends upon the hole shape and pattern (e.g., k = 0.263 for hexagonal, close-packed holes), and a_e, d and s are defined in Figure 3 and Equation 2. The collimator's efficiency determines the number of gamma ray counts that may be recorded for a given source distribution of radioactivity in a given scan time (often called count sensitivity). Since both the relative statistical noise (pixel value standard deviation) in the image, and the precision with which activity may be quantified decrease (improve) as the square root of the number of image counts, collimator efficiency is an important consideration. Note that either shortening the collimator hole length a or decreasing the septal thickness s increases the collimator efficiency, while decreasing the hole size d decreases the efficiency. In most practical situations the sensitivity will degrade approximately as the square of the geometric resolution.

Focusing Collimation. When imaging activity distributions smaller than the FOV of the gamma camera, significant performance gains may result from magnifying the object distribution to fill more of the camera's FOV. This can be accomplished by using fanbeam collimators [e.g., Jaszczak et al. (*13*)], which are quite useful for SPECT applications. Fanbeam collimators focus in one dimension to a focal line parallel to the axis of rotation of the gamma camera on the other side of the patient. (The reconstruction procedure for SPECT is then quite similar to that used for fanbeam CT scanners). Astigmatic collimators, which focus to two different focal lines in the two orthogonal directions, and cone-beam collimators, which focus to a point, may also be used for SPECT (*14*); however, projection data from these types of collimators are incompletely

sampled, which can result in image distortions when reconstructing with linear reconstruction algorithms (*15*).

When using a fanbeam collimator, the object magnification causes the geometric and intrinsic resolutions, both defined in the object plane, to improve in comparison to parallel-hole collimation (*16*). The exact transfer function of converging hole collimators was derived by Tsui and Gullberg (*17*). The fanbeam count sensitivity at any given distance is increased approximately by the ratio of the linear extent of the source viewed by the collimator at that distance to the extent of the same source against the collimator face. This means that for a point source in air, the sensitivity of a fanbeam collimator increases as the source is moved away from the collimator, whereas, that of a parallel-hole collimator is independent upon distance.

Septal Penetration and Scatter. Septal penetration and collimator scatter are two effects which can also affect quantitative accuracy, especially when imaging radionuclides with higher energies and/or multiple photopeaks. Both of these processes will broaden the PSF, thereby degrading contrast and quantitative accuracy. An analytic expression for the septal penetration contribution to the collimator PSF has not been developed, however, several investigators have successfully used numerical ray-tracing methods to examine the penetration component (*18–20*). Most collimator designers have used an ad hoc rule allowing a certain small fraction of gammas to penetrate along the minimum path length (see "w" in Fig. 3) through a single septum (*21,22*). Of course, the allowable penetration fraction should ultimately be dictated by the imaging or quantitative task we are trying to accomplish.

An analytic or numerically available description of the collimator scatter component has eluded researchers. de Vries et al. (*23*) used Monte Carlo simulation to show that the total collimator scatter contribution for a low-energy, general-purpose collimator is ~1.9% using a 20% energy window placed symmetrically about the ^{99m}Tc photopeak. Collimator scatter is a greater concern when imaging low- or medium-energy isotopes which also emit higher energy contaminant photons, such as ^{123}I or ^{111}In. These higher energy photons can scatter in the collimator, lose energy and be detected in a desired lower energy window of the gamma camera.

Gamma Camera and Readout Electronics. The gamma camera and associated electronics can also influence the quantitative capabilities of the SPECT system. The thickness of the NaI(Tl) crystal, for example, alters the tradeoff between count sensitivity and spatial resolution, although this effect is certainly not as pronounced as the tradeoff imposed by collimator selection. Perhaps more importantly, camera (and collimator) nonuniformities, if not adequately corrected, have been demonstrated to cause ring artifacts in reconstructed SPECT images (*24*). Even if the nonuniformities appear to be adequately corrected in selected planar images, it is quite important for SPECT imaging to make sure that there is no angular dependence to the required uniformity correction.

The energy resolution of the gamma camera affects the degree to which primary gamma photons may be separated from Compton scattered photons. The size and position of the pulse-height-analyzer energy window (or windows) is also critical. For example, a wide photopeak window yields images with more counts (hence, a better precision for activity estimations). The fraction of scattered photons, however, is also higher, which degrades spatial resolution and contrast, thereby adversely affecting the accuracy of activity and size estimates. Conversely, a narrow energy window would improve the accuracy of estimates at the expense of precision. Asymmetric energy windows, or multiple energy-window acquisition in combination with an appropriate software scatter compensation, may be used to improve quantitative accuracy significantly with minimal or no loss of precision. Of course, any such method relies upon a camera's ability to perform excellent linearity correction throughout the portion of the spectrum used by the method.

Finally, one should anticipate the effects of camera deadtime before undertaking a quantitative SPECT study. Pulse pileup could affect quantitative capabilities in different ways. Absolute quantitation would be difficult because the relationship between counts and activity at high count rates becomes nonlinear and, in the extreme, double-value (i.e., two different activities, one very high and one low, could give the same observed count rate). In addition, the mispositioning of events caused by two different gamma photons interacting almost simultaneously in two different crystal locations could significantly degrade spatial resolution by pulling the calculated event positions. Deadtime values for gamma camera systems are typically in the range 2–10 μsec, depending upon the manufacturer's electronics, source scatter geometry, and selected energy windows (*25*). For a 5-μsec deadtime, 10% of the counts are lost at a count rate of about 2×10^4 cps. For accurate quantitative work, we believe that the maximum count rate should be limited to about 5×10^4 cps, provided that an appropriate deadtime correction is used after image acquisition.

Display System. Since most quantitation schemes require use of the counts in different ROIs which are often drawn manually with a joystick or a mouse on a computer display screen, the display system becomes an important consideration. For example, the image should be displayed large enough so that the smallest desirable ROIs can be easily drawn by the viewer. Related to this, the response of the screen cursor to movements of the drawing device should be adjusted appropriately so that the cursor does not move too fast or too slow. Finally, the selection of the display brightness and contrast (window and level) can significantly affect the observer's decision about the location of boundaries. In general, automated or semi-automated boundary calculations on image data are to be preferred, when possible, for this reason.

Reconstruction Methods. The two most important limitations of SPECT data are those imposed by attenuation and poor statistics. Limitations in collimator resolution and

image degradation due to scatter follow close behind. Any balanced approach must consider not just one, such as attenuation, but all of these limitations. An important contribution to overall image degradation is the nonisotropic response of the camera to a point source as a function of distance. Concerning attenuation correction, it is necessary to consider the type of correction (uniform or nonuniform) and the region of the body to be imaged (cranium, thorax, abdomen).

Decay Methods. To account for the total activity involved in a given examination, it is necessary to perform decay correction on an image or image sequence. Generally, the intent is to correct for the physical decay of the radionuclide in question, since the biological effects are generally not known and in many instances are part of the question to be answered.

QUANTITATION METHODS

Patient Factors

The strength of nuclear medicine is its ability to perform functional studies using biological tracers. A primary limit, however, in the ability to perform quantitation is the information available from the patient, i.e., the accuracy of the model which describes the biokinetic distribution of the radiopharmaceutical. The biokinetic distribution is affected by human physiology and the properties of the pharmaceutical. For example, liver uptake is quite high for many pharmaceuticals by the very nature of the function of the liver. One example relates to labeled monoclonal antibodies; as fragments break down, the liver scavenges the fragments and thus the radionuclide. The lack of specificity of uptake implies that only a fraction of the pharmaceutical is extracted by the organ of interest. Cerebral blood flow indicators, for instance, result in an extraction of only a few percent of the agent (e.g., for HMPAO the extraction is about 5%) (*26*). Myocardial perfusion scans are also limited by the biokinetics because of poor extraction of the tracer.

Currently, there are many radiopharmaceuticals available and considerable research is under way for the development of others. In the majority of cases there is a lack of specificity for the organ or tumor of interest. This results in poor contrast and statistics for the study; therefore, it is necessary that the technical, procedural and reconstruction methods are optimized. Efforts are under way to have a national facility for developing new radionuclides which can provide better opportunities for improving the target specificity of the tracers. Although one can expect some improvements in the compounds available, human physiology is quite complex and organ systems are interrelated in such a way that specificity of uptake will probably remain relatively poor in the near future.

Technical Factors: Instrumentation

It is clear that multi-camera systems are currently state-of-the-art for SPECT studies. In addition to the versatility which they offer for a variety of imaging procedures, such systems, compared to single-head rotating cameras, provide a much higher count sensitivity for the same spatial resolution or, alternatively, a better spatial resolution for the same count sensitivity. Moreover, for small FOV studies, additional performance gains result from the use of converging fan-beam or cone-beam collimators.

Optimal Choice of Collimator Design Parameters for Quantitation. Isotope energy is the most important factor in selecting the collimator. Once an isotope has been selected it is then advisable to select the collimator with the highest resolution for the selected isotope. The tradeoff between resolution and sensitivity is not the dichotomy it once was (*27*). For instance, if one uses a low-resolution collimator to obtain a high count rate, then one may end up using some sort of resolution recovery scheme to improve the resolution. These restoration algorithms have one feature in common: they apply an average Gaussian-shaped collimator response function to the image, whereas the true collimator response function varies over the image. If scatter is removed, the image statistics will also be reduced. Therefore, if the result of an image with reduced counts and nonlinear noise amplification is induced by the restoration algorithm, it can be argued that the use, instead of a high-resolution collimator for image acquisition, would result in a better and more accurate image of the activity distribution with a simpler noise structure.

Fanbeam and conebeam collimators have demonstrated potential by offering improved resolution and sensitivity tradeoff when compared to parallel collimation, at the cost of a smaller FOV. The reduced FOV stems from the magnification produced by the collimator. Practical conebeam scanning with a Picker SX300 camera (Bedford Heights, OH) required the use of a special nonplanar orbit (*28,29*). The imaging characteristics of conebeam collimators also require use of special reconstruction algorithms to handle the different imaging geometry. In addition, the problem is confounded for conebeam collimation by the fact that a standard circular orbit or coplanar orbit does not meet the sufficiency condition which defines the data sampling required to permit an accurate tomographic reconstruction (*30*). The algorithms and the hardware necessary for clinically practical, quantitative conebeam SPECT are, therefore, still active areas of research.

It is evident from Equations 2, 4, and Figure 3 that a variation in any one geometric collimator parameter affects resolution and efficiency in different ways. For example, given a fixed septal thickness and hole size, increasing the collimator thickness, a, will improve the spatial resolution while decreasing the collimator's efficiency. Therefore, collimator design consists of determining the optimal tradeoff among these various performance parameters for a given task to be accomplished by the imaging procedure.

A somewhat simplistic optimization, first described by Keller (*21*), has been used by many collimator designers and discussed in some review articles. In his technique, three conditions are used to determine the three collimator geometric parameters (a, d, s). Assuming that the desired

spatial resolution is specified at an appropriate distance from the collimator and that a given probability of single-septal penetration (e.g., 1%) is considered acceptable, then the third constraint is obtained by maximizing the geometric efficiency. It is important to keep in mind the assumptions and limitations of this method. First, the procedure does not take into account the detailed shape of the point spread function or its components, but rather, treats only the FWHM of the geometric component and the fraction of allowed single-septal penetration. Second, collimator scatter is not included at all (in practice, this may be a significant concern only when imaging certain isotopes). Finally, it is assumed that the optimal spatial resolution and septal penetration fraction are already known for the appropriate imaging task.

A more sophisticated approach to collimator optimization which is directly relevant to the problem of quantitation from nuclear medicine images was recently addressed by Mueller et al. (*31*). These authors used a maximum-likelihood (ML), least-squares fitting program to estimate lesion parameters (amplitude and size) and background activity from image data, and compared this technique to the more traditional method of simply calculating the average and standard deviation of the total counts in a user-defined ROI on the images. The ML estimate was accurate for all lesion sizes. For lesions of a size less than 1.5–2.0 times the FWHM of the PSF, the ROI estimate was highly inaccurate, yet more reproducible (precise) than that of the ML estimate, as expected. A figure-of-merit was defined as the standard error of each fitting parameter, expressed as a percentage of the true (known) parameter value. By varying the FWHM of the PSF, and assuming that the pixel noise variance increases with the square of the FWHM, these authors determined that the optimal collimator resolution for estimating lesion amplitude corresponded to a FWHM of approximately 0.4 times the lesion diameter. This requirement on resolution results primarily from fitting for lesion size, as well as activity and background activity levels. In fact, the resolution that optimized the precision of the estimates of lesion size in this three-parameter estimation problem was only about 0.25 times the disk diameter.

Although the actual ML estimator described by Mueller et al. (*31*) may be impractical for clinical imaging (because it assumes that the image is describable by a very simple geometric model), it nevertheless provides a useful tool for system design optimization. The results of this study indicate that quantitative studies will often benefit from the use of a manufacturer's highest resolution collimator, especially with a multi-head SPECT system. Madsen et al. (*32*) recently demonstrated that the optimal spatial resolution (for minimizing the mean-squared error) may be as small as 4–5 mm FWHM for SPECT brain imaging of ^{99m}Tc-labeled radiopharmaceuticals with a multi-detector system. When fewer counts were available, e.g., when using a single-head SPECT instrument, the resolution that provided the minimum mean-squared error was about 6–7 mm FWHM.

There are several collimator design considerations that are especially important for SPECT. In planar projection images, the image noise is spatially uncorrelated from pixel to pixel. The statistical noise in tomographically reconstructed images is spatially correlated by the ramp filter used for reconstruction (*33,34*). For such correlated noise, the noise power spectrum (NPS) is not white (constant), but rather, varies as a function of spatial frequency. In SPECT, nonstationary projection noise and attenuation compensation procedures also influence the shape of the NPS (*35*). This is important to bear in mind for quantitation because parameter estimation from image data will benefit from prior information about the expected noise correlations.

It is clear that for a given collimator-detector combination, the best spatial resolution will be obtained when the collimator is as close to the patient as possible so that b in Equation 2 is minimized. This motivated the development of special cutoff gamma camera heads to clear the patient's shoulders for brain SPECT (*36*), as well as parallel slant-hole collimators (*37*) which permit angling the camera with the same consequences. The advent of SPECT systems with multiple (rectangular) heads and/or converging collimators has limited the application of these types of camera/collimator modifications primarily to single-headed systems.

Because the spatial resolution of a collimator worsens linearly with distance from the collimator, reconstructed SPECT images usually demonstrate a nonuniform reconstructed spatial resolution, e.g., the resolutions in the circumferential and radial directions are significantly different. The three-dimensional PSF may be made somewhat more stationary and isotropic by taking the conjugate mean of opposing projections before reconstruction (*38*), which is often done as an integral part of various attenuation compensation procedures. In addition, several reconstruction algorithms which compensate for this geometric nonstationarity have been recently described. The degree of nonstationarity over the tomographic FOV can also be reduced somewhat by increasing the bore length (a in Eq. 2) of the collimator.

Camera Systems. For the best possible quantitative capabilities, today's state-of-the-art camera systems should be able to image using energy window(s) placed asymmetrically around the photopeak without causing energy-dependent nonlinearities or nonuniformities. For SPECT, the uniformity should be corrected to about 1% (*23*), especially in the central FOV. This normally requires camera flood acquisitions of >30 million counts in a 64 × 64 matrix. The position and energy corrections should also be effective for all projection angles. These precautions will minimize the possibility of ring artifacts in SPECT images (*24*) and will allow the use of several different approaches to scatter correction which utilize multiple energy windows.

The energy resolution and the intrinsic camera spatial resolution should be as good as possible. For ^{99m}Tc, most current SPECT instrumentation provides an energy reso-

lution better than 10% and an intrinsic spatial resolution better than 3.5 mm. In addition, SPECT systems should be able to accommodate the expected count rates with minimal dead time or count rate loss. Because SPECT system manufacturers are moving toward providing collimators with better spatial resolution and, therefore, lower efficiency, this relaxes the count-rate requirements of the camera system because the count rate decreases approximately as the square of the improvement in collimator resolution (the FWHM of the PSF) considerably. The count rate per detector for a SPECT brain scan of 20 mCi of ^{99m}Tc-HMPAO with high-resolution collimators is about 5000 cps. At this counting rate, even a camera system with a rather large dead-time of 10 μs would record ~95% of the true counts. Finally, the PMT high voltage and pre-amplifier gains should either be stable for a week or longer (to permit relatively infrequent uniformity calibrations) or controlled with auto-tune techniques.

Procedural Factors

Optimized Imaging Parameters. The system resolution of a contemporary multiheaded SPECT system with a high-resolution collimator can be quite good. Close to the camera face, a FWHM of 6 mm is not unusual. The planar image pixel size is determined by the dimensions of the planar image and the zoom factor. The reconstructed image pixel size is determined by the factors which determine the planar image size as well as such factors as distance between the patient and the collimator and type of collimator. According to the sampling theorem of signal processing, one should select the pixel size to be no larger than one-half the dimension of the smallest detail that can be resolved by the camera (*39*). Also, as long as none of the views contain truncated projections, the zoom factor should be as large as possible, because there is no advantage to imaging empty space. As a rule of thumb, it is better to select a pixel dimension that is too small. A pixel dimension that does not meet the requirements of the sampling theorem (too large) will result in planar images that are aliased. This aliasing will be amplified in the reconstruction as artifacts.

The number of views or projection angles can have a critical effect upon SPECT quantitation. Obviously, one must have a certain number of projections, since one projection is sufficient to reconstruct objects only with circular symmetry, two views 90° apart are sufficient to reconstruct an object that varies as the cosine of the projection angle, and so on. Too many projection angles, however, result in planar images with reduced counts, so it appears as if there is a tradeoff between the number of views and the noise level in each view. From first principles, why should we expect a planar projection image that is optimal for planar imaging to be optimal for tomography? Certainly the overall noise level is important. The overall constraining factor in SPECT is total image time, both to minimize patient motion and to require that scanning time be short compared to the biological half-life of the functional agent. In the discussion below, we will present an objective means to determine the optimal number of projections for a given imaging situation.

The decision of whether to use continuous scanning versus step-and-shoot depends upon the efficiency of the gantry in cycling between images in the step-and-shoot mode and the number of projections desired. If the total cycling time is less than about 10% of the total scan time, then not much is lost, and much may be gained using the step-and-shoot mode. The continuous scan mode data are rebinned into projections, and the error introduced by rebinning the continuous scan mode data over a large included angle is not well understood. On the other hand, if large numbers of projections are desired, there is much less error introduced by rebinning continuous mode data, and the amount of time required for cycling in the step and shoot mode becomes prohibitive. The current trend is in the direction of more, rather than fewer projections, so continuous mode scanning may be the method of choice. It should be noted that the angular sampling size also depends on the size of the reconstructed image pixel.

As previously cited, there are a variety of factors that determine the quality of a SPECT image. These factors include pixel size, zoom factor, desired level of resolution, number of views, patient size and scanning time. In addition, these factors are also interrelated, some are more important than others. With conventional SPECT, scanning time is the limiting factor in most cases. Current experience indicates that the signal-to-noise ratio (S/N) of the reconstruction is most directly affected by the total counts in the sinogram. The number of angles will depend upon the camera resolution and the size of the patient, or equivalently, the distance from the axis of rotation to the ROI. The larger the patient, the more views will be needed. To accomplish this while keeping the overall scan time to a reasonable interval, one can reduce the time for each view. The planar projections may look too noisy, but the reconstructions need not reflect this. An operating principle that is beginning to emerge is that projection data that are optimal for quantitative SPECT are not necessarily optimal for a planar study. For 360° SPECT, the optimal number of projections that will prevent angular aliasing in the reconstruction is:

$$N \geq \pi D/\delta x, \qquad \text{Eq. 5}$$

where N is the # of projection angles in 360°, D is the diameter of the FOV (or diameter of a circle enclosing the region of interest) and δx is smallest linear dimension that can be resolved by the camera (*40–42*). Of course, the pixel size should also be less than $\delta x/2$. Using fewer projections may result in radial streaks at the periphery of the reconstruction, but it should be kept in mind that reconstruction algorithms vary somewhat in their robustness to angular undersampling. Also, the type of restoration filtering used will have an effect upon the minimum number of angles.

With the availability of nonstationary Fourier noise filters, satisfactory compensation for the nonstationary noise of radionuclide images is possible. Therefore, the total counts per pixel or even total counts per planar image is not as crucial a factor for quantitative imaging as it once was. Thus, it is probably best to select the pixel size that satisfies the sampling theorem. One can be sure that the aliasing resulting from a mismatch between pixel size and FWHM would propagate as artifacts into the reconstruction. The reduced counts in each planar projection, however, will affect a count dependent two-dimensional Metz or Wiener filter, causing the filter to use a lower cutoff frequency, thereby causing a loss of resolution recovery. One possible solution is to retune the filter for more resolution recovery. A more satisfactory answer is possibly to filter afterwards with a three-dimensional count/image-dependent Metz or Wiener filter, but the noise energy spectrum of the reconstructed SPECT image is not well understood and is an area of active research. Glick (*43*) and Moore (*35*) have studied the noise energy spectrum of SPECT reconstructions.

Elliptical Orbits Versus Circular Orbits. Everything else being equal, the orbit that follows the patient's contour is probably the best. With this type of orbit, camera resolution is optimized as is count rate. While camera manufacturers provide the ability to use contour-following orbits as well as elliptical and circular orbits in many cases, the resulting images using contour orbits are not necessarily better. It has been reported in the literature that circular orbits are better than elliptical orbits for ^{201}Tl cardiac SPECT (*44*). Other studies, e.g., Keyes (*45*) have not supported this conclusion. Improvement in SPECT resolution and image quality with contour-following orbits or elliptical orbits is dependent upon the quality of the reconstruction algorithm in conjunction with the stability of the SPECT cameras gantry and collimator design. For example, spatially variant detector response will cause artifacts in the reconstructed images if elliptical or contour-following orbits are used.

Calibration. Until recently, the most important problem in reproducibility was the mechanical and electronic stability of the imaging system. With a well-tuned SPECT system, the only QC measurement that needs to be done with each scan is a sensitivity measurement. Center of rotation measurements, uniformity floods and linearity checks may be done weekly or at longer intervals. Some other measurements, such as z-axis (long-axis) alignment, depend on the system, and whether the heads rotate. Here the judgment of the physicist responsible for QC and the recommendations of the manufacturer are crucial. Some other measurements, such as camera resolving time, can be made at still longer intervals.

Sensitivity measurements, on the other hand, can vary by as much as 10% on a daily basis even in the most carefully regulated environment. Since none of the other factors vary substantially, it is possible to update a calibration factor obtained from initial phantom studies by updating the sensitivity measurement (*40,46*).

The foundation for quantitative SPECT is QC and calibration. The routine aspects of calibration are becoming easier as hardware improves. Calibration for quantitative SPECT is an exhaustive process that begins with resolving time measurements and ends, if at all, with quantitative measurements of radionuclide concentration in phantom studies and validation with animal studies and patient biopsies.

Iterative and Noniterative Algorithms

Reconstruction and image restoration in SPECT may be performed in a number of ways. Two broad lines of approach have emerged which we refer to as the iterative and noniterative algorithms.

In essence the reconstruction problem involves solving:

$$P_i = \sum_j W_{ij} Y_j, \qquad \text{Eq. 6}$$

where P_i is the projection data for a single slice at an angle I, Y_j is the activity in cell j of an image and W_{ij} is the contribution of pixel (j) to the projection (i).

The W_{ij} represents for a given projection only the cells in the true image along a straight line across the image at an angle (i) will contribute to P_i. Thus, W (weighting factors) will depend on the interpolation since the projection lines will be at angles to the true image and entire pixels will not be in the projection path. For a given interpolation scheme, the W are constants.

The noniterative routines provide an analytical solution to the above problem. Filtered backprojection is a member of this class of solution.

If one considers the problem further, it can be understood that the counts emitted at some position do not necessarily make it to the detector position i, i.e., photons can be scattered, attenuated, absorbed by the collimator, not detected, etc. It is possible to take these conditions into account with:

$$P_i = \sum_j C_{ij} Y_j. \qquad \text{Eq. 7}$$

The C_{ij} represent the weighting factors discussed above in addition to the physics of the problem and are thus associated with the probability that a photon at a given cell (j) in the image will make it to the detector at some position (i) and be registered in that projection. In essence the model of scatter and detector response as well as attenuation processes is put into the problem. The C_{ij} are constants for a given image set. A solution to the problem is obtained through an iterative process for the desired true distribution of activity Y.

The iterative approach to solving ill-posed problems is found in many disciplines and is based on the tried-and-true approach of discretizing the fundamental equations as a system of linear equations. The basic premise of all iterative algorithms is the process to match the measured

image projections to the estimated projections. The estimated projections are determined from an initial reconstruction and are compared to the original data. The differences between the two datasets is used to correct the estimated projections. This cycle is repeated until the difference between the original projections and the estimated projections is smaller than some desired limit.

The maximum likelihood-expectation maximization (ML-EM) and the conjugate gradient (CG) methods are the most notable of these iterative techniques. The ML-EM algorithm uses the maximum likelihood technique to maximize the expected value for a given cell; that is, find the best average value taking into account the statistical fluctuations involved. Poisson statistics are ideally suited for the maximum likelihood process and thus, the ML-EM technique has a good statistical and physical basis for the solution of the reconstruction process. It possesses other desirable characteristics, such as nonnegativity of iterates and a less approximate model of photon noise than the chi square statistic. In addition, the iterative methods can incorporate a model of scatter and detector response as well as compensate for uniform attenuation. On the other hand, a high price is paid on two accounts: (a) it is slow to converge and (b) it is sensitive to the initial solution. One might reasonably expect a robust iterative method to be relatively insensitive to the initial solution. Then, a relatively close image obtained by filtered backprojection could be refined by ML-EM, but because of the persistence phenomenon, this is not possible—the artifacts of the filtered backprojection image persist as well. The only initial guess that seems to work consistently well with ML-EM is the flat image (BMW Tsui, *personal communication*; 1991) (*47*). The CG method, on the other hand, while not endowed with such attributes as nonnegativity, converges a great deal faster than ML-EM.

Noniterative algorithms are less frequently used in the solution of ill-posed problems. Most often, the problem does not lend itself to this treatment; the mathematical description of the problem is often too complex for existing techniques of analysis. Intrinsically, these methods are computationally efficient, though not particularly easy to code. For SPECT, the noniterative algorithms of current interest are the so-called intrinsic algorithms that are based on the exact solution for uniform attenuation within a convex body. This list includes the circular harmonic transform (CHT), the Bellini algorithm, exponentially-weighted filtered backprojection (EWBP), the Schneiberg CHT algorithm and the Tanaka algorithm.

Filtered backprojection itself is often used as a zeroth estimate of the radionuclide distribution in SPECT, it is also the most important noniterative reconstruction method as it is the basis for reconstruction algorithms in clinical use. It is quantitative only if there is negligible attenuation of the source distribution. A uniform disk of activity within a uniform attenuation medium of the same shape is reconstructed with filtered backprojection in

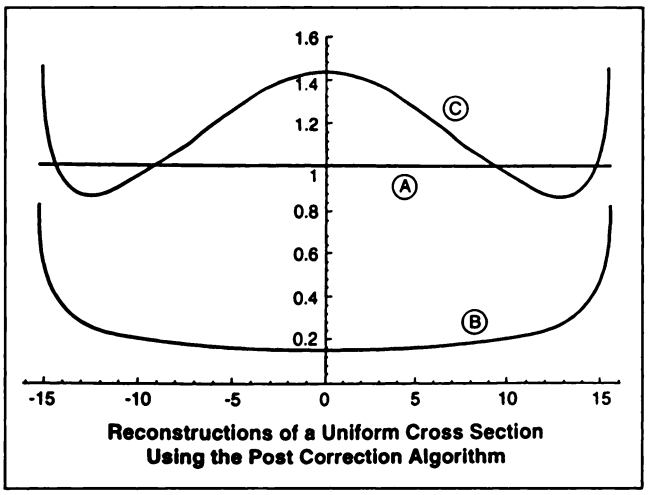

FIGURE 4. Reconstruction of a uniform cross section using the postcorrection algorithm. (A) A uniform cylinder of diameter 30.7 cm. (B) Reconstruction without attenuation. (C) The postcorrection algorithm applied to (B). Attenuation coefficient = 0.147 cm^{-1}.

Figure 4. The overall effect is to underestimate the source distribution. Filtered backprojection involves three steps:

1. Fourier transform of the projection sinogram with respect to the slice coordinate.
2. This transformed projection is multiplied by a ramp filter and inversely transformed back to sinogram space.
3. These filtered projections are finally backprojected.

According to the central slice theorem (*48–50*), the one-dimensional Fourier transform of the projection data maps out the two-dimensional Fourier transform of the object on a polar grid. Thus, the three steps of filtered backprojection are equivalent to the two-dimensional inverse Fourier transform of the object. The ramp filter can be physically interpreted as the area function for converting the rectilinear pixels of the one-dimensional Fourier transform of the projection data to polar pixels of the two-dimensional Fourier transform of the object.

There is no general agreement whether any of the algorithms mentioned can be used alone as an element of a reconstruction protocol for quantitative SPECT. Two of these algorithms, CHT and Bellini, are based on the energy-distance principle (EDP). The EDP allows for a frequency space interpretation of attenuation, spatially-varying collimator resolution, scatter and noise. Although the Bellini algorithm has been described as a preprocessing method, it is mathematically identical to the CHT with EDP (*50*). These methods, however, have not been used to compensate for nonuniform attenuation to date.

Reconstruction/Compensation Methods

Attenuation. The most important physical factor affecting SPECT is the attenuation of photons in the body. The extent of photon attenuation can be appreciated from the fact that the half-value layer for 140 keV photons through soft-tissue is on the order of 4.5 cm for narrow beam

geometry. If not compensated for, the reconstructed image will be quantitatively inaccurate when compared to the actual object distribution and in some cases may generate undesirable image artifacts and distortions. Thus, accurate compensation for photon attenuation is essential in SPECT image reconstruction and processing. Together with compensation for other physical factors such as scatter and response function of the detector system, we can obtain high fidelity SPECT images for improved clinical diagnosis and accurate estimation of radioactivity in vivo.

In SPECT, the attenuated radon transform, which includes the effect of photon attenuation, is given by:

$$p(r, \theta) = \int_{-\alpha}^{+\alpha} ds\, f(x, y) \exp\left\{ - \int_{0}^{L(x,y)} dl\, \mu(u,v) \right\}, \quad \text{Eq. 8}$$

where f(x, y) represents the object distribution at location (x, y) and p(r, θ) represents the projection data at angle θ and position r, μ(u, v) is the attenuation coefficient at position (u, v), and L(x, y) is the distance from the point (x, y) to the detector along the projection ray.

The goal of all attenuation compensation methods is to seek a solution for the attenuated radon transform given in Equation 8 such that an accurate estimate of the object distribution f(x, y) can be obtained. An analytic solution for the general form of Equation 8 is difficult and has not been found (*51*). Practical attenuation compensation methods can be grouped into two general categories. In the first category, an assumption is made that the attenuation coefficient throughout the portion of the body to be imaged is uniform, i.e. μ(u, v) = μ is a constant. The second category of attenuation methods address situations where the attenuation distribution in the body is nonuniform.

Compensation Methods for Uniform Attenuation. The assumption of uniform attenuation can be applied to imaging of the head and abdomen areas where most body constituents are soft-tissue types with similar attenuation coefficients. Compensation methods for uniform attenuation can be divided into three general classes, namely preprocessing, intrinsic and postprocessing methods, according to its application before, during and after reconstruction, respectively.

Preprocessing Methods. In preprocessing methods, attenuation compensation is applied to the projection data before reconstruction (*52–54*). Typically, these methods make use of conjugate counting techniques which have been used in quantitative measurement of radioactivity in vivo using conventional nuclear medicine imaging techniques (*55*). The methods assume that the radioactivity within the source is uniformly distributed and the attenuation coefficient is constant throughout the body. The geometric mean of the conjugate views is largely dependent on the body thickness, weakly dependent on the source thickness, and independent of source depth. On the other hand, the arithmetic mean is largely dependent upon body thickness and weakly dependent on source thickness and source depth.

The geometric mean and arithmetic mean compensation methods are easy to implement and work well for a single radioactive source in a uniform attenuating medium. The drawbacks of preprocessing methods occur in situations where multiple sources are involved and knowledge of source thickness and source depth is required. The geometric mean method tends to give connecting count density between isolated radioactive sources in the reconstructed image. The arithmetic mean method shows decreased count density towards the center of the reconstructed image, indicating the dependence of source depth.

The preprocessing method proposed by Bellini (*56*) compensates for attenuation by appropriately shifting and smoothing the Fourier transform of the sinogram of the projection data. The reconstructed image is quantitatively accurate even for multiple sources and without the problems associated with the geometric mean and arithmetic mean compensation methods (*57*).

Intrinsic Methods. With intrinsic compensation methods, a solution for the attenuated radon transform given in Equation 8 is derived for uniform attenuation, i.e., μ(x, y) = μ is a constant, of a convex-shaped medium (*58 and King MA, personal communication*, 1991). The compensation method involves multiplying the projection data with an exponential function whose exponent is a function of body thickness, filtering with a modified ramp filter in the frequency domain, and backprojecting the filtered projections with an exponential weighting. The modified ramp filter is the same as the regular ramp filter, except that its value is zero in the frequency range between zero and $\mu/2\pi$.

The intrinsic compensation method is simple to implement and works well even for multiple sources. It tends, however, to amplify noise in the projection data onto the reconstructed image. Application of a smoothing filter is necessary to control for the reconstructed image noise (*58*). Furthermore, the modified filter can be designed to smooth out noise and to reduce image distortions (*59*).

Postprocessing Method. In the postprocessing method proposed by Chang (*60*), the measured projection data are first reconstructed without attenuation compensation. A correction factor is calculated at each image point as the average attenuation factor over all projection angles. For uniform attenuation, knowledge of the average attenuation coefficient and of the body contour is required. For nonuniform attenuation, the correction factor can be calculated from the known attenuation distribution. The reconstructed image is multiplied by the correction factors to compensate for attenuation. The compensation method tends to overcorrect some parts and undercorrect others of the image, especially when the object consists of an extended source. An iterative scheme is proposed to improve the accuracy of the compensation.

The Chang algorithm is exact for a single point source. As the source distribution becomes larger, the error be-

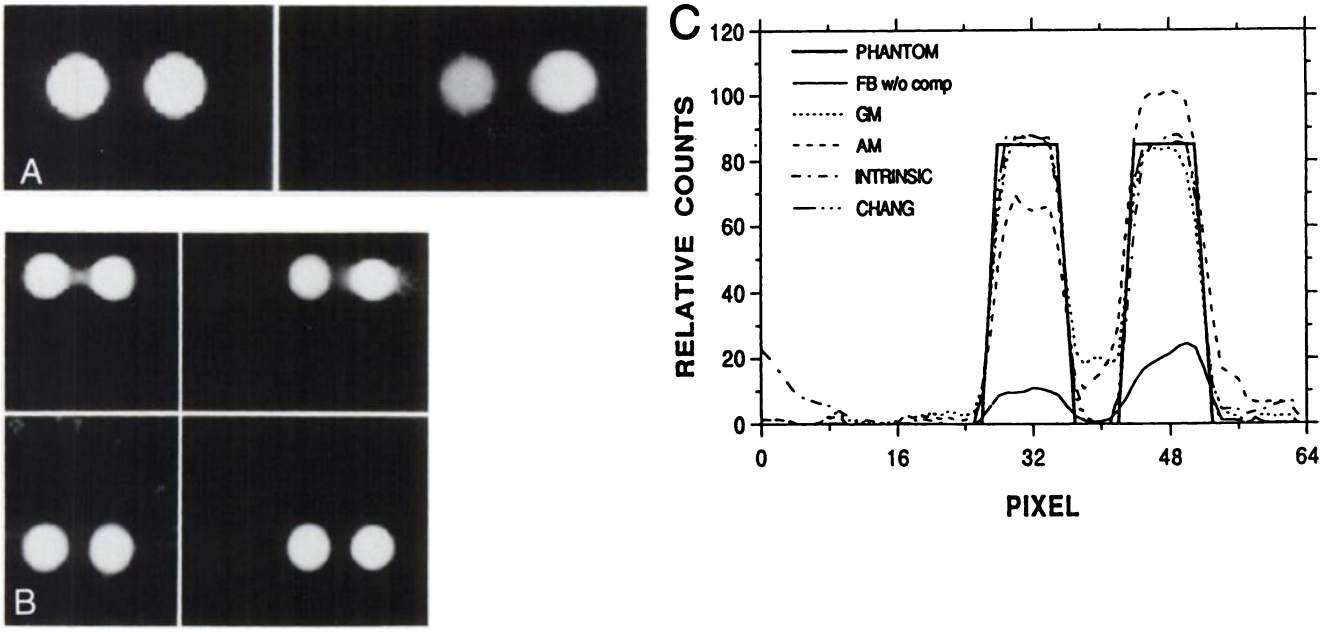

FIGURE 5. Simulation study demonstrating the effectiveness of various uniform attenuation compensation methods. (A) Left phantom image of radioactivity distribution and (right) reconstructed image obtained from the FB method without attenuation compensation. (B) Reconstructed images obtained from preprocessing methods using geometric mean (upper left) and arithmetic mean (upper right) techniques, (lower left) the intrinsic method and (lower right) the postprocessing method. (C) Profiles through the centers of the radioactive sources of the reconstructed images in (B).

comes serious. For a uniform disk of activity in a uniform attenuating medium of the same shape, the error at the center is about 40%, and the error at the edge is about 60%, going to infinity (the postcorrection algorithm has a singularity at the edge of the uniform disk). The edge artifact is reduced by the blurring effect of the SPRF (Fig. 4). This figure was based on both an analytical solution and simulation for the post correction algorithm and the source-attenuator distribution. The analytical solution is based on the continuous limit (arbitrarily small pixel sizes and continuous scanning). So as resolution in SPECT imaging systems improves, the error will become more apparent. Of course, one may use the iterated post correction method, but noise is amplified in a reconstruction that is somewhat noisy to start with. The postcorrection method, however, often yields good qualitative information, especially for focal distributions, and good contrast for cold lesions, because the uncorrected image, which is reconstructed without attenuation, is count poor, so cold lesions are fairly accurately imaged, provided that these lesions are not surrounded by large areas of relatively high background activity.

In general, the postprocessing compensation method performs well for uniform attenuation situations. With noisy data, this method tends to amplify image noise at high iteration numbers. Also, the method produces image features which fluctuate with the iterative number. For these reasons, no more than one or two iterations are recommended.

Figure 5 shows the results from a simulation study demonstrating the effectiveness of various uniform attenuation compensation methods. The simulated phantom consists of two 5.75 cm diameter circularly shaped uniform sources of ^{99m}Tc embedded in a 35-cm diameter circularly shaped uniform attenuating medium. The centers of the circular sources are positioned at the center and 9.5 cm off-center of the attenuating medium. The projection data are noise-free and are generated, including the effects of the uniform attenuating medium and a high-resolution collimator, at a radius-of-rotation of 17.5 cm. There are 128 projection views over 360°. The images are reconstructed in 64 × 64 matrices. The left image in Figure 5A shows the phantom image of radioactivity distribution and the right one shows the reconstructed image obtained from the filtered back-projection method without attenuation compensation, indicating the degree of inaccurate quantitation.

Figure 5B shows reconstructed images obtained from preprocessing methods using the geometric mean (upper left) and arithmetic mean (upper right) techniques, the intrinsic method (lower left), and the postprocessing method (lower right). Figure 5C shows profiles through the centers of the radioactive sources of the reconstructed images in Figure 5B.

In general, the compensation methods provide good quantitative accuracy. The arithmetic mean method presents the most uneven radioactivity distribution between the two sources, presumably due to the dependence of source depth in the compensation algorithm. In the recon-

structed image obtained from the geometric mean method, the highest connecting count density between the isolated sources is found. The intrinsic compensation method depicts image artifacts towards the edge of the image even in the noise-free case. The postprocessing method provides a good reconstructed image with some unevenness over the flat part of the radioactive source distribution.

Compensation Methods for Nonuniform Attenuation. Compensation methods for nonuniform attenuation are important in SPECT imaging of the heart and lungs where the thoracic region consists of muscle, bone and lung tissues, each with different attenuation coefficients. Since an analytic solution of the attenuated Radon transform is unavailable, compensation methods in this situation involve approximation schemes or iterative reconstruction methods (*60–73*). Also, knowledge of the attenuation coefficient distribution through experimental measurement is necessary.

An effective method to compensate for nonuniform attenuation is the Chang algorithm which includes the attenuation distribution in the calculation of the correction factor (*49,67–71*). The advantage of the compensation method is its fast processing time. Overall good quantitative accuracy can be obtained in one iteration. The method tends to produce image features which vary with iteration and enhanced image noise at high iteration numbers (*70*).

Another approach to compensating for nonuniform attenuation in SPECT is the use of a new class of reconstruction methods which utilize iterative algorithms. These algorithms are derived from statistical criteria and estimate the reconstructed image from the measured projection data using parameter estimation techniques. Examples of iterative reconstruction algorithms include the ML-EM (*74,75*), WLS-CG (weighted least squares with conjugate gradient) (*76*) and MAP-EM (maximum a posteriori with expectation-maximization) (*77*) algorithms.

A projector and backprojector pair are required in the iterative reconstruction method. By modeling the imaging process in the projector and backprojector pair, image degrading factors such as photon attenuation, detector response function and scatter can be compensated accurately. For example, the exact attenuation map through the patient can be incorporated into the projector and backprojector pair (*66*) for accurate compensation of nonuniform attenuation in liver and cardiac SPECT imaging (*67,72,73*) and in tumor dosimetry calculation (*78*). A projector and backprojector pair which model both attenuation and detector response has been shown to provide improved quantitative accuracy, spatial resolution and decreased noise in the reconstructed image (*73*).

The iterative reconstruction methods are inherently computationally intensive. Each iteration step consists of a projection and a backprojection step requiring about twice as many computations as the filtered backprojection algorithm. Projectors and backprojectors which model the imaging process require even more calculations. Furthermore, multiple iterations are necessary to achieve satisfactory reconstructed image quality. The exact number of iterations required depends upon the convergence properties of the particular iterative algorithm in use (*71*). Advances in the development of iterative algorithms and computational hardware have brought these iterative reconstruction methods close to clinical use.

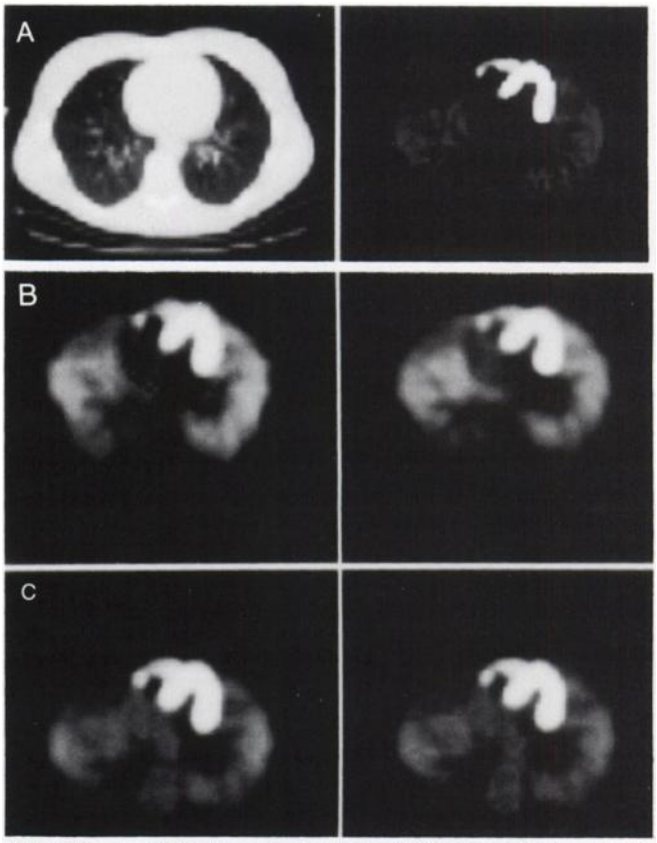

FIGURE 6. Simulation study demonstrating the effectiveness of various nonuniform attenuation compensation methods. (A) Left image: simulated phantom derived from a patient CT image of the cardiac-chest region and transformed into attenuation coefficient distribution of ^{201}Tl for use in the image reconstruction. Right image: Simulated ^{201}Tl uptake in the myocardium and lungs. Noisefree emission projection data are generated, including the effects of the nonuniform attenuation distribution and a general-purpose collimator at a radius-of-rotation of 22.5 cm. (B) Reconstructed images obtained with: (upper left) the FB method without attenuation compensation, (upper right) the Chang algorithm assuming uniform attenuation within the body contour, (lower left) the Chang algorithm using nonuniform attenuation distribution in (A) and (lower right) the iterative ML-EM algorithm which incorporates the nonuniform attenuation distribution in the projection-backprojection process. (C) Horizontal profiles through the center of the heart of the reconstructed images in (B).

Figure 6 shows the results from a simulation study demonstrating the effectiveness of various nonuniform attenuation compensation methods. The attenuation distribution shown in the left image of Figure 6A is derived from a patient's cardiac-chest region CT image and transformed into attenuation coefficient distribution of ^{201}Tl for use in the image reconstruction. The right image in Figure 6B shows the simulated ^{201}Tl uptake in the myocardium and lungs. The noise-free emission projection data are gener-

ated, including the effects of the nonuniform attenuation distribution and a general-purpose collimator at a radius of rotation of 22.5 cm. There are 64 projection views over 180° (45° LPO to 45° RAO) with reconstruction in 64 × 64 matrices.

Figure 6B shows the reconstructed images obtained from various reconstruction and compensation methods. Figure 6C shows the horizontal profiles through the center of the heart of the reconstructed images in Figure 6A. In Figure 6A, the image in the upper left is obtained from the filtered background algorithm without attenuation compensation indicating the degree of inaccurate quantitation. The image in the upper right is obtained from the Chang algorithm assuming uniform attenuation within the body contour. The image depicts the resulting image quality when the simplistic but inaccurate assumption about the attenuation distribution is used. The images in the lower left and lower right are obtained from the Chang algorithm after one iteration and the iterative ML-EM algorithm after 100 iterations, respectively, both utilizing the nonuniform attenuation distribution in Figure 6A. The images demonstrate the generally high quantitative accuracy obtained from the attenuation compensation methods.

The Energy Distance Principle. The EDP, or frequency distance relationship, is a novel and useful approach to SPECT reconstruction and image processing. It is based on Fourier analysis and the CHT. One first reorganizes the SPECT projections into sinograms. A sinogram is a two-dimensional angle-slice image of the projection data in which a point source traces out a sine wave. A slice containing multiple point sources will generate a sinogram that is the superposition of many sine waves. Next, one takes the two-dimensional Fourier transform of the sinogram with respect to the projection angle and the slice coordinate. Because of the periodic nature of the sinogram with respect to angle, we have to take care to get the correct numerical implementation of the Fourier transform (*52*). Results are best if zero fill is not used in the application of the FFT with respect to projection angle. The resulting transform is the circular harmonic transform. The Fourier transform with respect to the slice variable is a transform of nonperiodic data. We call this special case of the two-dimensional Fourier transform the CHT-FT of the sinogram.

This algorithm makes use of interpolation in both frequency space and projection space. Interpolation is accomplished efficiently by the use of FFT interpolation, which did not come into existence until the early 1980's (*79*). The EDP was not recognized until the mid 1980's in the pioneering work of Edholm et al. (*80*). Since that time, it has been applied to various problems in SPECT, including the development of spatially-variant Fourier transform restoration of spatially-varying collimator resolution (*81*), determining missing projections for hexagonal PET detector arrays (*51*) and the CHT algorithm with EDP (*40,52*). Without the use of the EDP, the CHT algorithm is equivalent to and as sensitive to noise as the EWBP. With the EDP, the exact solution is retained but S/N in the reconstructed image is improved by a factor of three. This translates into an improvement in sensitivity by a factor of nine.

In the techniques for the deconvolution of collimator blur, the CHT-SPECT and Bellini algorithms all utilize the translation variant approach to Fourier transform image reconstruction and restoration.

SCATTER

In addition to the methods just discussed to develop quantitative SPECT imaging, one further correction that must be implemented is scatter. Apart from iterative methods which can, in principle, incorporate a scatter correction, most other attenuation methods do not handle scatter and therefore do not provide exact compensation to generate a correct quantitative reconstruction of SPECT data. To correct for scatter, various techniques have been proposed based on assumptions concerning the characteristics of the scatter radiation. These assumptions were made to derive efficient methods to correct for scatter.

Stationary Assumption. The easiest and fastest method to correct for scatter is the use of a stationary assumption. In the stationary assumption, the scatter is assumed to be both analytically defined and also not dependent on the source distribution of radioactivity, variations in the scattering material, source position in the scattering medium and position (distance and angle) of the detector (camera head). Scatter is likewise assumed to be linear with respect to the source strength.

The stationary assumption provides an easy framework in which to apply simple scatter correction algorithms which are fast; however, this assumption breaks down for complex sources or attenuation distributions. The quantitative images produced can vary widely in their accuracy (10%–45%) and probably do not approach the truth for the determination of tissue activity in most clinical cases.

Current methods using the stationary assumption for scatter correction include the use of dual-window techniques and convolution and deconvolution techniques, (e.g., Tanaka's algorithm (*62*), Makai et al. (*82*). The dual-window techniques [e.g., Jaszczak et al. (*83*), Manglos et al. (*84*), Koral et al. (*85*), Gilardi et al. (*86*)] make the assumption that if a window is chosen in a region below the nonscattered data window, the activity within this window is due solely to scatter. Making the stationary assumption, then, it is assumed that a fraction of the activity measured in this window, k, can be subtracted from the photopeak window to correct for scatter. The value of k is considered constant in this model. The number of counts subtracted from the photopeak window will be proportional to the counts collected within the scatter window. As the amount of scatter within a system increases, the number of counts within the scatter window will also increase. Typical values of k are 0.4 to 0.6. This implies that 40%–60% of the counts in the photopeak window is due to scatter.

Problems with the dual-window technique include the

assumption that k is constant. In actuality, k should change as a function of angle around the patient, the distance from the source to the surface of the patient and the tissues between the source and the surface of the patient. The scatter properties of different tissues can vary by 20%–50%. Because of this, the dual-window technique is generally considered unsuitable for scatter correction for quantitative purposes. It will, however, improve image contrast.

The convolution techniques by Tanaka et al. (*62*) and Yanch et al. (*87*) are limited by the assumption of stationarity. The convolution methods, however, do a more exact modeling of the human body and can be iterative, which improves the quality of scatter correction. The convolution techniques apply a model for scatter compensation in coordinate space. The technique uses a model/mathematical formula which describes the correction needed using coordinate space not directly dependent upon the frequency.

The deconvolution techniques remove scatter from the image data by making assumptions concerning the characteristics of scatter for a particular camera system and patient. For example, the photopeak PSF will be assumed to be Gaussian in shape, but the scattered PSF will not and, in addition, will have a shape dependent upon the depth of the source. By creating a model for the shape of the nonscattered and the scattered PSF and using deconvolution techniques, the model hopes to remove scatter from the data. This technique does assume that the scatter is well behaved and that the scattering material is uniform throughout the patient.

In general, the stationary assumption models provide a quick and easy method to correct for scatter, but the models are not very accurate. These models are best for improving image quality if quantitative imaging is not necessary, but ease of use and speed are important.

Nonstationary Assumption. The nonstationary assumption for scatter is a more realistic scatter mode. In this case, the scatter is assumed to be dependent upon source locations, object size, detector angle, etc. The model used is not an exact representation, but is more sophisticated than the stationary assumption. The use of this type of model produces a better scatter correction, but in most cases the results still do not match the actual distribution precisely.

Various methods/models have been developed under the nonstationary assumption. These include the use of asymmetric dual-energy windows, a modification of the dual-window technique, Koral et al. (*88*), Gaussian subtraction method (*89*), Ljungberg's method (*90,97*) and holospectral imaging (*92*) among others such as factor analysis of dynamic structures (*93,94*). In addition, energy specific correction algorithms have been developed to determine the amount of scatter from the energy spectra and use this data to correct for scatter (*95*).

The asymmetric dual-energy windows are a modification of standard dual-windows techniques. The modification includes the use of an asymmetric window for the nonscattered energy peak. By shifting the window to the high energy side of the decay peak, scatter is reduced in this window. Residual scatter is removed by using a lower energy scatter window which is not necessarily the same size as the nonscatter window. By using the asymmetric window, scatter is removed in a manner which is dependent upon source geometry and object size.

The modified dual-window technique (*88*) is basically the same as described under the stationary assumption, except that the value of k can vary as a function of angle around the patient. The value of k can also depend on other parameters, which makes the model more dependent on patient characteristics.

The Gaussian subtraction technique (*89*) is based on the fact that if no scatter is present, the energy peak for an isotope should be basically Gaussian in shape. In this model, a Gaussian function is fitted to the high energy side of the emission peak. The parameters determined for the Gaussian function are used to determine the number of good counts within the standard 15% or 20% energy window.

A technique similar to the Gaussian subtraction technique is the dual-photopeak window method developed by King et al. (*96*). This technique is also based on the hypothesis that the lower part of the photopeak will contain a significant amount of scatter, while the upper energy portion of the photopeak will be relatively scatter free. This technique estimates the ratio between two nonoverlapping energy windows which cover the photopeak to determine the scatter fraction. The scatter fraction is determined as:

$$SF = AR_s^B + C, \qquad \text{Eq. 9}$$

where SF is the scatter fraction, A, B and C are determined by regression analysis from calibration studies and R_s is the ratio of corrected counts in the lower energy window divided by the upper window. The resulting scatter fractions are used to correct the standard SPECT images for scatter compensation. Examples of the effectiveness of scatter compensation are shown in Figures 7–9. In each of these figures the application of scatter compensation has improved image quality, particularly contrast; quantitative accuracy, however, is estimated to be 15%.

Holospectral imaging (*92*) is another technique based on an analysis of energy spectra. This technique is an energy-space method which uses principal-component analysis to attempt to separate scattered from unscattered photons. This technique is more computationally intensive than the Gaussian subtraction technique and, in addition, allows the use of photons lower than the emitted energy which have not scattered within the patient but within the NaI(Tl) crystal or collimator to be accepted, thereby potentially improving precision. The use of multiple energy windows, however, may provide practical problems for implementing this method with many of today's gamma cameras, which are unable to correct for linearity and energy separately in many different energy windows.

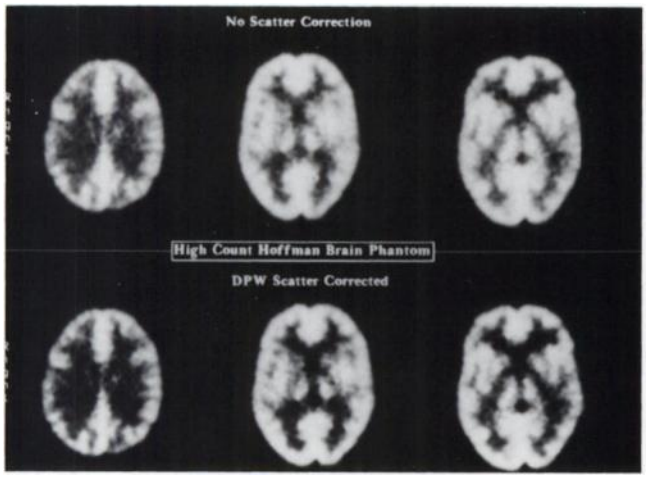

FIGURE 7. Example of the effect of scatter compensation. Three slices through the Hoffman brain phantom. Images are uncorrected on top and corrected at bottom. Images scatter compensated using the method of King. The same three-dimensional post Butterworth correction is applied to both images with order 4.0, cutoff 0.3 and a pixel size of 2.7 mm. Images were acquired with a pair of 7.5% windows abutted at the photopeak of ^{99m}Tc.

The final nonstationary model to be described is the Ljungberg method (*90,91*). This technique corrects for scatter by using Monte Carlo simulated scatter line-spread functions. The model simulates line-spread functions for scatter as a function of position within a phantom or subject. By using a reconstructed emission image to determine source positions, the amount of scatter is estimated from the simulations. The estimated scatter contribution is subtracted from the projection data prior to attenuation correction and reconstruction. The authors report accuracies within ±10% of true activities.

FIGURE 8. Rollo phantom images using the same acquisition and processing parameters (A). Four different contrasts and four different size spheres are placed in a water bath with 12.7 cm water in front of the phantom. (Left) No scatter compensation, image. (Right) Scatter compensation using the method of King.

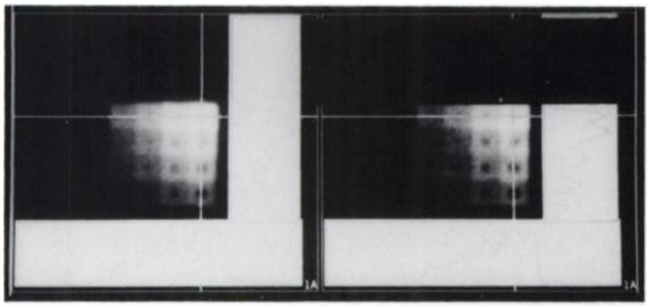

FIGURE 9. Same images as in Figure 8 but with vertical and horizontal activity curves through the spheres to demonstrate differences in contrast. (Figures 7–9 provided by Michael A. King, PhD, University of Massachusetts).

In general, the nonstationary models are more exact than the stationary models for producing better images, e.g., more accurate contrast and better quantitation. How well these models reproduce the truth for tissue activity still needs to be determined for clinically realistic distributions. The disadvantages of these models are the increased complexity to apply them and increased processing time. In addition, models such as Holospectral imaging and Gaussian subtraction also require the use of multiple-energy windows.

Experimental Methods. One experimental system has been marketed by Siemens Gammasonics (*97,98*) (WAM technique) to attempt scatter correction in real time. This method, which is a pseudo nonstationary model, determines a weight based on energy for each photon detected. Photons whose energies are at or above the emission energy are given weights greater than one and those with energies less than the emission energy are given weights less than one. In some cases, the weights from low-energy photons can be negative.

This technique will correct for the number of scattered events and will therefore improve image contrast. Its ability to determine true tissue activity is unknown. This technique, because of its weighting of the spectra, fits a nonstationary approximation.

Exact Nonstationary Assumptions. Finally, the last general method for scatter compensation is the exact nonstationary assumption model. Models based on this principle try to compensate for scatter by minimizing the use of simplifying assumptions and model the scatter interactions from first principles. As a class, these techniques are based on iterative solutions and incorporate the physics of the interactions between photons and the scattering material or will use the magnitude and shape of the scatter function as a starting point. In addition, they make no assumption as to the geometry involved. Therefore, these models will compensate for scatter more accurately, but with more complexity and increased computation.

The basic method for the exact models is the simultaneous compensation for attenuation and scatter with reconstruction. The source activity for each pixel will be determined by using all projections which can affect that particular pixel simultaneously. In these methods, a priori knowledge of the source distributions is not necessary but knowledge of the patient boundary (body contour), attenuation distribution and imaging system characteristics are required, e.g., knowledge of collimator divergence and energy resolution.

Examples of two methods that use this exact nonstationary assumption are Floyd's inverse Monte Carlo method and the Frey and Tsui methods (*99–101*), along with an older, yet similar method by Msaki et al. (*102*).

The inverse Monte Carlo method (*103,104*) uses Monte Carlo techniques to estimate the amount and shape of scatter from a known source distribution, scattering object size and configuration. Monte Carlo algorithm models the physics of Compton scatter and collimator divergence and potentially coherent scatter; the algorithm can also model the interactions of the source and scattered photons with the camera collimator and NaI crystal. The inverse Monte Carlo method is primarily based upon modeling the SPECT system's characteristics using Monte Carlo techniques. This includes energy resolution, radius of rotation, etc. The resulting set of linear equations is used to solve for the activity distribution (image).

The inverse Monte Carlo model differs from the Ljungberg method by exactly modeling the object size and scatter properties along with actual source distributions. The Ljungberg model estimates line spread functions to estimate the scatter contribution. Both methods will improve image contrast and both will provide tissue activity. The inverse Monte Carlo model will, however, perform better because it estimates the amount of scatter for each case properly, whereas the Ljungberg method estimates average scatter contribution only for a class of objects. It should be noted, however, that the inverse Monte Carlo method is slow since Monte Carlo calculations need to be performed for each case.

The method of Frey and Tsui uses a predetermined scatter response function to correct for scatter in a projector-backprojector pair iterative solution. This method uses a slab derived scatter estimation to model the asymmetric and the spatially variant scatter response function in uniformly attenuating systems. The primary advantage of this method is that scatter counts are not thrown away as in other methods with the consequential increase in noise. This method tries to return scattered photons to their original trajectory, thus improving contrast without increased noise. Another advantage of this method is that Monte Carlo simulations do not need to be performed for each object imaged. The use of the spatially variant scatter response function will provide better quantitative reconstruction of SPECT images. It can be applied to any source and object geometry with a convex shape. The initial results of this technique show that its estimation of the scatter response function is close to that predicted by Monte Carlo calculations for simple phantom geometries. In one case with actual phantom data, the error between the counts within a source from actual data to the ML-EM algorithm with the slab derived scatter functions is small.

This method does have the potential, along with other techniques, to improve quantitation in SPECT imaging. One other drawback to this technique is that the time per iteration is still too long for clinical use, but this should not be a factor in the future.

Processing Methods: Edge Detection

Many nuclear medicine procedures rely on the determination of boundaries that divide or segment an image into regions that are of specific diagnostic importance. Most commonly, these boundaries are associated with the edges of the radionuclide distribution and define a closed region from which volumes or activity quantitation is obtained. Obtaining these edges is at the heart of the segmentation process and the various methods can be classified by rules used to define the edges. An early discussion of several approaches originally developed for planar imaging which were later extended to SPECT is given by Cahill (*105*). Some specific applications of edge determination in SPECT include the determination of left ventricular volume, ejection fraction and mass (*106,107*), measuring infarct size and mass (*108–110*), determination of the anatomical boundaries for attenuation correction (*111–114*), the determination of volumes for three-dimensional treatment planning for internal radionuclide therapy planning and management (*115*) and for three-dimensional surface and volume display which enhances the visualization of physiological information (*116*). Boundary determination is also assuming an important role in multimodal image registration in which knowing the spatial extent of an ROI is essential to registering the images and correlation of anatomical and functional information (*117*). The three-dimensional characteristics of SPECT allow for a more natural approach to segmentation of regions of the body. The ability to extract specific tomographic planes from the reconstructed images that contain the region to be examined improves segmentation by removing the influence of superimposed activity. Algorithms can then be restricted to operate on the specific region in question. The same technical limitations that degrade image quality influence the accuracy of image segmentation methods (*118*).

The most common applications of segmentation to SPECT images is for the determination of the volume of a region or the estimation of the activity contained within a volume. Volume determination is three-dimensional by definition and therefore SPECT is well suited for this application. Volume information can be obtained from the set of two-dimensional tomographic planes by determination of the edges on each plane and subsequent stacking of successive ROIs to generate the VOI. This approach is limited since information about the edges in directions out of the tomographic plane is not available. Recently, three-dimensional segmentation algorithms have been investigated for SPECT which attempt to use the information from adjacent planes in determining boundaries (*119,120*). This approach is logical since it matches the three-dimensional characteristics of SPECT and exploits all the available data.

Volume quantitation reduces to determining the number of voxels belonging to the region to be quantified. The number is then multiplied by the unit voxel volume to obtain the total volume. This approach limits the possible volume values to a multiple of the unit volume. More sophisticated methods attempt to improve upon this approach by use of interpolative background corrections to improve the accuracy of quantitation (*121,122*). Interpola-

tion accounts for the partial volume effect in which the voxel value contains a weighted sum of counts from the different classes of object intersecting the voxel, which can include no object of interest (*123*). If activity quantitation of an organ or lesion is the desired objective, the measured value is still ultimately dependent upon a volume determination. Once defined, the counts are summed within the volume and related to the activity through a calibration protocol.

Edge determination methods for volume and activity quantitation in SPECT can be broadly classified as manual or operator-defined, semi-automated and automated. Manual methods have historically served the needs of most procedures but have many limitations (*110*). These procedures are time-consuming and are subject to inter and intra-operative variations which compromise reproducibility and objectivity. The results are also dependent upon imaging system limitations such as variable resolution, acquisition protocol, noise and reconstruction protocol. For objects containing significant activity and isolated from surrounding sources or surrounded by sources of relatively low activity, quantification of counts or volume determination is less sensitive to boundary errors than when surrounding activity obscures the object. For example, increasing the radius of a ROI which encompasses an isolated source beyond the true boundary will affect the measured counts minimally as only background is added. This is less true for sources of low source-to-background ratios. If significant adjacent or underlying activity is present, counts from these regions can spill into the ROI due to the limited spatial resolution of the imaging system. This consideration is often reflected in the design of imaging protocols which attempt to produce an optimal target-to-background activity ratio for improved detection and boundary determination.

Semi-automated methods require some intervention by the operator, including reducing the search to the immediate region of the object of interest. Once defined, an automated computational algorithm searches the region using its specific criteria to find the boundaries or produces a new quantity at each pixel that can be used in further processing to obtain the edges. Thresholding (*124*), modified thresholding methods (*125*) and methods related to derivative operations (*120,126*) are the most commonly applied semi-automated techniques. Thresholding implies that the voxels belonging to the object of interest can be segmented from the image based on the magnitude of the measured counts at the voxel or the magnitude of some quantity derived from the counts at the voxel such as a thresholding of a gradient image. A commonly used computational device for separating voxels based on the magnitude of counts is the gray-level histogram (*125,126*). In this approach, the number of voxels with a given gray-level (counts) are plotted against the gray-level values. Hopefully, a value or values can be found which separate the voxels into discrete regions, thereby identifying voxels to be quantified. In this way, boundaries are determined by an on or off assignment of the voxels based on the cutoff criteria. The problem with this method is that count information alone is generally not sufficient to segment various regions accurately. Also, the physical factors that affect image quality greatly affect the shape of the histogram making segmentation from this relationship for a broad range of imaging scenarios difficult at best. A more sophisticated group of methods known as adaptive gray-level histogram techniques uses statistical methods applied to the histogram to determine an optimal critical value for thresholding (*127*).

Typically, computationally determined boundaries will be displayed on a reference image for acceptance or rejection by the operator. Most commercial imaging systems allow the interactive modification of boundaries after automated definition or the assignment of new search parameters to improve the results. This fact reflects the limited ability of current automated methods to perform accurately under a variety of imaging conditions. As a result, there is currently no single method which works for a broad range of studies and specific methods have been developed for application to a given study type.

Derivative-based methods are a computational approach that use information related to the rate of change of the radionuclide distribution to locate and segment regions of the image. Examples include the gradient operator, Laplacian, Sobel, and Robert's operators (*122*). In general, these are computational algorithms that convert the image into a new set of values (one for each voxel) related to the rate of change of the count values. It assumes that regions where count values change most rapidly are associated with edges or boundaries of various regions. The methods related to first-derivatives of the image require specification of a further criterion such as a threshold value for segmentation. The second-order derivative operations (e.g. Laplacian) use the maximum rate of change of the first derivative as the criteria for edge definition (*122*) and therefore also require operator intervention and are semi-automated methods.

RECOMMENDATIONS

In this review of quantitative imaging for SPECT, we have provided a comprehensive discussion of the mechanisms responsible for degrading SPECT images and methods to improve both image quality and quantitation. It is possible that the reader might feel that it is not easy to properly correct images for attenuation and scatter from reading this report or that it might not be worth the effort.

We would have to disagree with this sentiment. The effective implementation of attenuation correction and some scatter compensation can improve image quality, e.g., image resolution and contrast significantly. Because of this, it is important to correct SPECT images. The degree to which any given clinical facility will implement attenuation correction and scatter compensation will depend upon upon the ability of personnel to develop these

correction procedures. This requires a complete understanding of the methods, their pitfalls, as well as the ability to verify the correct implementation of the chosen methods. This thought then leads to different recommendations for different nuclear medicine groups.

Ideally, it is always desirable to correct images for all errors to produce quantitative images. Realistically, this is not possible at this time. We would recommend that the amount of correction be based on a given facility's ability to detect errors in the compensation methods; most facilities should look first to improved image quality.

In general, it is highly advisable for all SPECT users to study their QA/QC procedures carefully with the aim to improve general image quality. It is also important for all users to look at the clinically available software and decide which reconstruction algorithms and which filters will provide the best diagnostic images for a particular study. The user will have to weigh their understanding of the various reconstruction algorithms and filter methods with the ability of their staff and systems to produce consistent high quality SPECT studies.

For small departments (with no physicist in-house and perform few SPECT procedures except for decay correction) it might not be prudent to perform any improvements at this time if the manufacturer does not provide a simple software procedure. The main thrust for these departments would be directed to excellent QA/QC of their systems, and urging equipment manufacturers to develop user-friendly, reasonable correction procedures. When departments have a physicist at their disposal and perform a significant number of SPECT procedures, correction for decay and attenuation should definitely be performed. Correction for scatter may follow one of the simpler techniques and the results should be improved image quality and, perhaps, quantitative accuracies of about 10%.

Research oriented departments with a basic science core should consider full attenuation correction and scatter compensation to produce quantitative images. These departments should have the expertise to fully understand the algorithms used and to be able to recognize their failures. The result should be not only improved image quality, but also true tissue specific activity for research studies.

Given these general recommendations, what are the actual techniques to be used? For small facilities with no physicist, the standard manufacturer's attenuation correction should be applied, e.g., Chang's algorithm. At this time, probably no other corrections should be applied to the data. Currently, however, a number of manufacturers are working to provide a nonuniform attenuation correction technique. At the time of writing this manuscript, one manufacturer has obtained FDA approval and others are in the process. These efforts primarily address the attenuation problem but not scatter. These techniques will undergo much testing and clinical validation.

ML-EM reconstruction algorithms with attenuation compensation methods can be used at facilities that have a physicist, but do not have a significant research group. Careful evaluation of the product is a must. Scatter compensation can be applied using one of the several techniques mentioned, e.g., King's method, dual-window, Gaussian subtraction. These methods will only improve image quality. Quantitative imaging is possible, but the robustness and reliability would have to be determined for each case.

Finally, for both basic and clinical research projects at facilities that have significant computational ability, use of the ML-EM reconstruction or equivalent is a must with scatter compensation applied. Scatter compensation can be applied with the nonstationary assumption methods for improved image quality, but for quantitative imaging, it is recommended that one of the exact nonstationary models be used. This is time consuming and difficult, but for accurate tissue characterization it is necessary at this time. This will also follow in-house verification of the algorithms used for quantitation.

It is to be expected as more research is completed in quantitative SPECT techniques that the more complicated reconstruction algorithms and scatter compensation techniques will become more robust and therefore be useful in less sophisticated clinics. Interestingly, manufacturers are currently marketing attenuation correction techniques based on measured patient attenuation maps. We would encourage readers to review the article by Tsui et al. (*128*) for more information on quantitative SPECT imaging.

CLINICAL CONSIDERATIONS

So far, we have concentrated on answering the question: What effects must be considered (and treated) to obtain images from which quantitative measures may be extracted? We have assumed that the measures of interest are usually volumes or counts per unit volume. The reader should be reminded, however, that these metrics are necessary but not sufficient for obtaining directly usable clinical results. For example, in several clinical procedures, one would usually like to know at least how many microcuries per cubic centimeter (or Bequerel/cubic centimeter) of activity are present in a given tissue. In addition to implementing a procedure which compensates appropriately for physical effects discussed in the previous sections, one must calibrate the sensitivity of the whole image acquisition and reconstruction process. In other words, one should perform an appropriate phantom study, using accurately measured activities, in an attenuator as similar as possible in size, shape and properties to a typical patient.

Even then, however, there may not be sufficient information to be of clinical utility. Consider SPECT imaging of regional cerebral blood flow (rCBF). Even if one knows the total activity injected into a peripheral vein of the patient and the total activity ending up in each cubic centimeter of the brain, this information alone is not enough to calculate rCBF (in this case, the arterial input concentration would also have to be determined).

In general, quantitative imaging might prove useful if all the required data are available and good statistics can be acquired. The required data includes not only quantitative SPECT images, but also appropriate input functions and/or model to describe the physiological properties of the pharmaceutical tracer used. At the least improved image quality should improve diagnosis.

CONCLUSION

In general, the most important contribution to SPECT that can be made by implementing various corrections is improved image quality. Accurate quantitation is also desirable but not easily obtainable by most departments. With future developments in methods to correct SPECT data (along with faster computer systems) data correction and quantitative SPECT will enter the clinical arena.

ACKNOWLEDGMENTS

Selected portions of the material on collimation are reproduced with permission from Moore et al. (*129*). The authors would like to acknowledge the support and encouragement, as well as the original idea for this project and article, of Tom Lewellen, PhD and the Computer and Instrumentation Council of the Society of Nuclear Medicine.

REFERENCES

1. Bevington PR. *Data reduction and error analysis for the physical sciences*. New York: McGraw-Hill; 1969.
2. Harris CC, Greer KL, Jaszczak RJ, Floyd CE, Fearnow C, Coleman RE. Technetium-99m attenuation coefficients in water-filled phantoms determined with gamma cameras. *Med Phys* 1984;11:681–685.
3. Katsnelson Y. *An introduction to harmonic analysis*. New York: Dover Publications; 1976.
4. Lanczos C. *Applied analysis*. New York: Dover Publications; 1988.
5. Prigent F, Hyun M, Berman D, et al. Effect of motion on thallium-201 SPECT: a simulation and clinical study [Abstract]. *J Nucl Med* 1990;31: 934.
6. Cooper JA, Neumann PH, McCandless BK. Effect of patient motion on tomographic myocardial perfusion imaging. *J Nucl Med* 1992;33:1566–1571.
7. Botvinick EH, Zhu YY, O'Connell, Dae MW. A quantitative assessment of patient motion and its effect on myocardial perfusion SPECT images. *J Nucl Med* 1993;34:303–310.
8. Anger HO. Scintillation camera with multichannel collimators. *J Nucl Med* 1964;5:515–531.
9. Mather RL. Gamma-ray collimator penetration and scattering effects. *J Appl Phys* 1957;28:1200–1207.
10. Gerber MS, Miller DW. Parallel-hole collimator design. *J Nucl Med* 1974; 15:724–725.
11. Muehllehner G, Dudek J, Moyer R. Influence of hole shape on collimator performance. *Phys Med Biol* 1976;21:242–250.
12. Metz CE, Atkins FB, Beck RN. The geometric transfer function component for scintillation camera collimators with straight parallel holes. *Phys Med Biol* 1980;25:1059–1070.
13. Jaszczak RJ, Chang LT, Murphy PH. Single-photon emission computed tomography using multi-slice fanbeam collimators. *IEEE Trans Nucl Sci* 1979;26:610–618.
14. Jaszczak RJ, Floyd CE, Manglos SH, Greer KL, Coleman RE. Conebeam collimation for single-photon emission computed tomography: analysis simulation and image reconstruction using filtered backprojection. *Med Phys* 1986;13:484–489.
15. Gullberg GT, Christian PE, Zeng GL, Datz FL, Morgan HT. Conebeam tomography of the heart using single-photon emission computed tomography. *Invest Radiol* 1991;26:681–688.
16. Moyer RA. A low-energy multi-hole converging collimator compared with a pinhole collimator. *J Nucl Med* 1974;15:59–64.
17. Tsui BMW, Gullberg GT. The geometric transfer function for conebeam and fanbeam collimators. *Phys Med Biol* 1990;35:81–93.
18. Muehllehner G, Luig H. Septal penetration in scintillation camera collimators. *Phys Med Biol* 1973;18:855–862.
19. Newiger H, Jordan K. Optimization of collimators for imaging positron emitters by a gamma camera. *Eur J Nucl Med* 1985;11:230–234.
20. Beck RN, Redtung LD. Collimator design using ray-tracing techniques. *IEEE Trans Nucl Sci* 1985;NS-32:865–869.
21. Keller EL. Optimum dimensions of parallel-hole, multi-aperture collimators for gamma ray cameras. *J Nucl Med* 1968;9:233–235.
22. Kibby PM. The design of multichannel collimators for radioisotope cameras. *Br J Radiol* 1969;42:91–101.
23. deVries DJ, Moore SC, Zimmerman RE, Mueller SP, Friedland B, Lanza RC. Development and validation of a Monte Carlo simulation of photon transport in an Anger camera. *IEEE Trans Med Imag* 1990;9:430–438.
24. Gullberg GT. An analytical approach to quantify uniformity artifacts for circular and noncircular detector motion in SPECT imaging. *Med Phys* 1987;14:105–114.
25. Sorenson JA, Phelps ME. *Physics in nuclear medicine*, 2nd edition. Philadelphia: W.B. Saunders Co., 1987.
26. Podreka I, Suess E, Goldenberg G, et al. Initial experience with technetium-99m HMPAO brain SPECT. *J Nucl Med* 1987;28:1657–1666.
27. Muehllehner G. Effect of resolution improvement on required count density in ECT imaging: a computer simulation. *Phys Med Biol* 1985;30:163–173.
28. Gullberg GT, Christian PE, Zeng GL, Datz FL, Morgan HT. Conebeam tomography of the heart using single-photon emission computed tomography. *Invest Radiol* 1991;26:681–688.
29. Esser PD, Jakimcius A, Foley L. The peanut orbit: a modified elliptical orbit for single-photon emission computed tomography imaging. *Med Phys* 1989;16:114–118.
30. Orlov SS. Theory of three-dimensional reconstruction. I. Conditions for a complete set of projections. *Sov Phys Crystallog* 1975;20:312–314.
31. Mueller SP, Kijewski MF, Moore SC, Holman BL. Maximum-likelihood estimation: a mathematical model for quantitation in nuclear medicine. *J Nucl Med* 1990;31:1693–1701.
32. Madsen MT, Chang W, Hichwa RD. Spatial resolution and count density requirements in brain SPECT imaging. *Phys Med Biol* 1992;37:1625–1636.
33. Riederer SJ, Pelc NJ, Chesler DA. The noise power spectrum in computed x-ray tomography. *Phys Med Biol* 1978;23:446–454.
34. Kijewski MF, Judy PF. The noise power spectrum of CT images. *Phys Med Biol* 1987;32:565–575.
35. Moore SC, Kijewski MF, Mueller SP, Holman BL. SPECT image noise power: effects of nonstationary projection noise and attenuation compensation. *J Nucl Med* 1988;29:1704–1709.
36. Larsson SA, Bergstrand G, Bergstedt H, et al. A special cutoff gamma camera for high-resolution SPECT of the head. *J Nucl Med* 1984;25:1023–1030.
37. Polak JF, Holman BL, Moretti JL, Eisner RL, Lister-James J, English RJ. Iodine-123 HIPDM brain imaging with a rotating gamma camera and slant-hole collimator. *J Nucl Med* 1984;25:495–498.
38. Glick SJ, King MA, Knesaurek K, Burbank K. An investigation of the stationarity of the three-dimensional modulation transfer function of SPECT. *IEEE Trans Nucl Sci* 1989;36:973–977.
39. Parker JA. *Image reconstruction in radiological imaging*, CRC Press 1990.
40. Hawkins WG, Yang NC, Leichner PK. Validation of the circular harmonic transform (CHT) algorithm for quantitative SPECT. *J Nucl Med* 1991;32: 141–150.
41. Jaszczak RJ, Coleman HE, Chun BL. SPECT. *IEEE Trans Nucl Sci* 1980;NS-27:1137–1152.
42. Huesman RH. The effects of a finite number of projection angles and finite lateral sampling of projections on the propagation of statistical errors in transverse section reconstruction. *Phys Med Biol* 1977;32:511–521.
43. Glick SJ, Penney BJ, King MA. Filtering of SPECT reconstruction made using Bellini's attenuation correction method: a comparison of three preconstruction filters and a postreconstruction Wiener filter. *IEEE Trans Nucl Sci* 1991;38:663–669.
44. Maniawski PJ, Morgan HT, Wackers FJT. Orbit related variation in spatial resolution as a source of artifactual defects in thallium-201 SPECT. *J Nucl Med* 1991;32:671–675.
45. Keyes JW Jr. SPECT and artifacts: in search of the imaginary lesion, [Editorial]. *J Nucl Med* 1991;32:875–877.
46. Leichner PK, Vreisendorp HM, Hawkins WG, et al. Quantitative SPECT for indium-111 labeled antibodies in the livers of beagle dogs. *J Nucl Med* 1991;32:1442–1444.

47. Tsui, BMW. Personal Communication; 1991.
48. Stark H, Woods JW, Indraneel P, Hingorani R. Direct Fourier reconstruction in computer tomography. *IEEE Trans ASSP* 1981;29:237–244.
49. Bracewell OF, Riddle BC. Inversion of fanbeam scans in radio astronomy. *J Astrophysical* 1967;150:417–434.
50. DeRosier DJ, Klug A. Reconstruction of three-dimensional structures from electron micrographs. *Nature* 1968;217:130–134.
51. Karp JS, Muehllehner G, Lewitt RM. Constrained Fourier space method for compensation of missing data in emission computed tomography, *IEEE Trans Med Imag* 1988;7:21–25.
52. Hawkins WG, Leichner PK, Yang NC. The circular harmonic transform for SPECT and boundary conditions on the Fourier transform of the sinogram. *IEEE Trans Med Imag* 1988;7;135–148.
53. Gullberg GT. The attenuated radon transform: theory and application in medicine and biology. PhD Dissertation, University of California at Berkeley, 1979.
54. Kay DB, Keyes JW. First order corrections for absorption and resolution compensation in radionuclide Fourier tomography. *J Nucl Med* 1975;16: 540–541.
55. Budinger TF, Gullberg GT, Huesman RH. Emission computed tomography. Herman GT, ed. In: *Topics in applied physics, image reconstruction from projections, implementation and applications*, New York: Springer-Verlag; 1979;147–246.
56. Bellini S, Piacentini M, Cafforia C, Rocca F. Compensation of tissue absorption in emission tomography. *IEEE Trans ASSP* 1979;27:213–218.
57. Sorenson JA. Methods for quantitative measurement of radioactivity in vivo by whole-body counting. In Hine GJ, Sorenson JA, eds. *Instrumentation in nuclear medicine*, vol. 2, New York: Academic Press; 1974:311–348.
58. Tretiak OJ, Delaney P. The exponential convolution algorithm for emission computed axial tomography. In: Brill AB, Price RR, eds. *Rev. Inform. Process. Med. Imaging*. Vanderbilt University, Nashville, TN; Oak Ridge National Laboratory Rep. ORNL/BCTIC-2, 1978;266–278.
59. Tretiak OJ, Metz CE. The exponential radon transform. *SIAM J Appl Math* 1980;39:341–354.
60. Chang LT. A method for attenuation correction in radionuclide computed tomography. *IEEE Trans Nucl Sci* 1978;NS–25:638–643.
61. Gullberg GT, Budinger TF. The use of filtering methods to compensate for constant attenuation in single-photon emission computed tomography. *IEEE Trans Biomed Eng* 1981;28:142–157.
62. Tanaka T, Toyama H, Murayama H. Convolutional image reconstruction for quantitative single-photon emission computed tomography. *Phys Med Bio* 1984;29:1489–1500.
63. Budinger TG, Gullberg GT. Three-dimensional reconstruction in nuclear medicine emission imaging. *IEEE Trans Nucl Sci* 1974;NS–21:2–10.
64. Walters TE, Simon W, Chesler DA, Correia JA, Riederer SJ. Radionuclide axial tomography with correction internal absorption. In: Raynaud C, Todd-Pokropek A, eds. *Information processing in scintigraphy*. Orsay, France: Comissairat a L'energie Atomique; 1976:333–342.
65. Moore SC, Brunelle JA, Kirsch C. Quantitative multi-detector emission computerized tomography using iterative attenuation compensation. *J Nucl Med* 1982;23:706–714.
66. Gullberg GT, Huesman RH, Malko JA, Pelc NJ, Budinger TF. An attenuated projector-backprojector for iterative SPECT reconstruction. *Phys Med Biol* 1986;30:799–816.
67. Malko JA, Van Heertum RL, Gullberg GT, Kowalsky WP. SPECT liver imaging using an iterative attenuation correction algorithm and an external flood source. *J Nucl Med* 1986;27:701–705.
68. Manglos SH, Jaszczak RJ, Floyd CE, Hahn LJ, Greer KL, Coleman RE. Nonisotropic attenuation in SPECT: phantom tests of quantitative effects and compensation techniques. *J Nucl Med* 1987;28:1584–1591.
69. Manglos SH, Jaszczak RJ, Floyd CE, Hahn LJ, Greer KL, Coleman RE. A quantitative comparison of attenuation-weighted backprojection with multiplicative and iterative post-processing attenuation correction in SPECT. *IEEE Trans Med Imag* 1988;7:127–134.
70. Manglos SJ, Jaszczak RJ, Floyd CE. Weighted backprojection implemented with a nonuniform attenuation map for improved SPECT quantitation. *IEEE Trans Nucl Sci* 1988;NS–35:625–628.
71. Tsui BMW, Hu HB, Gilland DR, Gullberg GT. Implementation of simultaneous attenuation and detector response correction in SPECT. *IEEE Trans Nucl Sci* 1988;NS–35:778–783.
72. Tsui BMW, Gullberg GT, Edgerton ER, Ballard JG, Perry JR, McCartney WH, Berg J. Correction of nonuniform attenuation in cardiac SPECT imaging. *J Nucl Med* 1989;30:497–507.
73. Tsui BMW, Zhao XD, Frey EC, Gullberg GT. Comparison between ML-EM and WLS-CG algorithms for SPECT image reconstruction. *IEEE Trans Nucl Sci* 1991;38:1766–1772.
74. Lang K, Carson R. EM reconstruction algorithms for emission and transmission tomography. *J Comp Assist Tomogr* 1984;8:306–316.
75. Shepp LA, Vardi Y. Maximum likelihood reconstruction for emission tomography. *Trans Med Imag* 1982;MI–1:113–122.
76. Huesman RH, Gullberg GT, Greenberg WL, Budinger TF. *User manual, Donner algorithms for reconstruction tomography*. Berkeley, CA: Lawrence Laboratory, University of California; 1977.
77. Levitan E, Herman GT. A maximum a posteriori probability expectation maximization algorithm for image reconstruction in emission tomography. *IEEE Trans Med Imag* 1987;MI–6:185–192.
78. Koral KF, Zasadny KR, Swallem FM, Buchbinder SF, Francis IR, Kaminski MS, Wahl RL. Importance of intra-therapy single-photon emission tomography imaging in calculating tumor dosimetry for a lymphoma patient. *Euro J Nucl Med* 1991;18:432–435.
79. Hawkins WG, Links JM, Leichner PK. FFT-based interpolation for arbitrary factorizations: applications to cross-sectional imaging. *Proceeding of 14th World Congress at Georgia Tech on Computational and App. Mathematics* 1994;2:724–726.
80. Edholm PR, Lewitt RM, Lindholm B. Novel properties of the Fourier decomposition of the sinogram. *SPIE Proc* 1986;671:8–18.
81. Lewitt RW, Edholm PR, Xia W. Fourier methods for the correction of depth dependent blurring. *SPIE Medical Image Processing III. Image Processing*. 1989;1092:232–243.
82. Makai T, Links JM, Douglass KH, Wagner HN Jr. Scatter correction in SPECT using nonuniform attenuation data. *Phys Med Biol* 1988;33:1129–40.
83. Jaszcak RJ, Floyd CE Jr, Coleman RE. Scatter compensation techniques for SPECT. *IEEE Trans Nucl Sci* 1985;NS–32:786–793.
84. Manglos SH, Jaszcak RJ, Floyd CE, et al. Nonisotropic attenuation in SPECT: phantom tests of quantitative effects and compensation techniques. *J Nucl Med* 1987;28:1584–1591.
85. Koral KF, Swailem FM, Buchbinder S, et al. SPECT dual-energy-window Compton correction: scatter multiplier required for quantification. *J Nucl Med* 1990;31:90–98.
86. Gilardi MC, Bettinardi V, Todd-Pokropek A, et al. Assessment and comparison of three scatter correction techniques in single-photon emission computed tomography. *J Nucl Med* 1988;29:1971–1979.
87. Yanch JC, Flower MA, Webb S. Improved quantification of radionuclide uptake using deconvolution and windowed subtraction techniques for scatter compensation in single-photon emission computed tomography. *Med Phys* 1990;17:1011–1022.
88. Koral KF, Wang X, Rogers WL, et al. SPECT Compton-scattering correction by analysis of energy spectra. *J Nucl Med* 1988;29:195–202.
89. Rosenthal MS, Henry LJ. Initial evaluation of a Gaussian scatter correction technique. *Int J Radiat Appl Instrum Part A [Appl Radiat Isot]* 1992;43:1123–1128.
90. Ljungberg M, Strand SE. Attenuation and scatter correction in SPECT for sources in a nonhomogeneous object: a Monte Carlo study. *J Nucl Med* 1991;32:1278–1284.
91. Ljungberg M, Strand SE. Scatter and attenuation correction in SPECT using density maps and Monte Carlo simulated scatter functions. *J Nucl Med* 1990;31:1560–1567.
92. Gagnon D, Todd-Pokropek A, Laperiere L, et al. Analysis of scatter, quantum noise and camera nonuniformity in nuclear medicine studies using Holospectral imaging [Abstract]. *J Nucl Med* 1989;30:807.
93. Mas J, Hannequin P, Ben Younes R, et al. Scatter correction in planar imaging and SPECT by constrained factor analysis of dynamic structures (FADS). *Phys Med Biol* 1990;35:1451–1465.
94. Mas J, Ben Younes B, Bidet R. Improvement of quantification in SPECT studies by scatter and attenuation compensation. *Eur J Nucl Med* 1989; 15:351–356.
95. Singh M, Horne C. Use of a germanium detector to optimize scatter correction in SPECT. *J Nucl Med* 1987;28:1853–1860.
96. King MA, Hademenos GJ, Glick SJ. A dual-photopeak window method for scatter correction. *J Nucl Med* 1992;33:605–612.
97. DeVito RP, Hamill JJ, Treffert JD, et al. Energy-weighted acquisition of scintigraphic images using finite spatial filters. *J Nucl Med* 1989;30:2029–2035.
98. DeVito RP, Hamill JJ. Determination of weighting functions for energy-weighted acquisition. *J Nucl Med* 1991;32:343–349.
99. Frey EC, Tsui BMW. Spatial properties of the scatter response function in SPECT. *IEEE Trans Nucl Sci* 1991;38:789–794.
100. Frey EC, Tsui BMW. Parameterization of the scatter response function in

SPECT imaging using Monte Carlo simulation. *IEEE Trans Nucl Sci* 1990; 37:1308–1315.
101. Frey EC, Tsui BMW. A practical method for incorporating scatter in a projector-backprojector for accurate scatter compensation in SPECT. *IEEE Trans Nucl Sci* 1993;40:1107–1116.
102. Msaki P, Axelsson B, Dahl CM, Larsson SA. Generalized scatter correction method in SPECT using point scatter distribution functions. *J Nucl Med* 1987;28:1861–1869.
103. Bowsher JE, Floyd CE Jr. Treatment of Compton scattering in maximum-likelihood, expectation-maximization reconstructions of SPECT images. *J Nucl Med* 1991;32:1285–1291.
104. Floyd CE Jr, Jaszczak RJ, Greer KL, Coleman RE. Inverse Monte Carlo as a unified reconstruction algorithm for ECT. *J Nucl Med* 1986;27:1577–1585.
105. Cahill PT, Ornstein E, Ho SL. Edge detection algorithms in nuclear medicine. *IEEE Trans Nucl Sci* 1976;NS-23:555–559.
106. Faber TL, Stokey EM, Templeton GH, Akers MS, Paekey RW, Corbett JR. Quantification of three-dimensional left ventricular segmental wall motion and volumes from gated tomographic radionuclide ventriculograms. *J Nucl Med* 1989;30:638–649.
107. Narahara KA, Thompson CJ, Maublant JC, Criley JM, Mena I. Estimation of left ventricular mass in normal and infarcted canine hearts using thallium-201 SPECT. *J Nucl Med* 1987;28:1315–1321.
108. Prigent F, Maddahi J, Garcia EV, Resser K, Lew AS, Berman DS. Comparative methods for quantifying myocardial infarct size by thallium-201 SPECT. *J Nucl Med* 1987;28:325–333.
109. Keyes JW, Brady TJ, Leonard PF, Svetkoff DB, Winter SM, Rogers WL, Rose EA. Calculation of viable and infarcted myocardial mass from thallium-201 tomograms. *J Nucl Med* 1981;22:339–343.
110. Johnson LL, Lerrick KS, Caromilas J, et al. Measurement of infarct size and percentage myocardium infarcted in a dog preparation with single-photon emission computed tomography, thallium-201 and indium-111 monoclonal antimyosin Fab. *Circulation* 1987;76:181–190.
111. Galt JR, Cullom SJ, Garcia EV. SPECT quantification: a simplified method of attenuation correction for cardiac imaging. *J Nucl Med* 1992;33:2232–2237.
112. Gullberg GT, Malko JA, Eisner RL. Boundary determination methods for attenuation correction in single-photon emission computed tomography. In: Esser PD, ed. *Emission computed tomography: current trends*. Reston, VA: Society of Nuclear Medicine; 1983:33–53.
113. Hawman EG. Impact of body contour on quantitative SPECT imaging. In: Raynaud C, ed. *Nuclear medicine and biology. Proceedings of the third world congress of nuclear medicine and biology, vol. 1*. Paris: Pergamon; 1982:1038–1041.
114. Hosoba M, Wani H, Toyama H, Murata H, Tanaka E. Automated body contour detection in SPECT: effects on quantitative studies. *J Nucl Med* 1986;28:1148–1191.
115. Sgouros G, Barest G, Thekkumthala J, Chui C, Mohan R, Bigler RE, Zanzonico PB. Treatment planning for internal radionuclide therapy: three-dimensional dosimetry for nonuniformly distributed radionuclides. *J Nucl Med* 1990;31:1884–1891.
116. Wallis JW, Miller TR, Lerner CA, Kleerup EC. Three-dimensional display in nuclear medicine. *IEEE Trans Med Imag* 1989;8:297–303.
117. Pelizzari CA, Chen GTY, Spelbring DR, Weichselbaum RR, Chen CT. Accurate three-dimensional registration CT, PET and/or MR images of the brain. *J Comput Assist Tomogr* 1989;13:20–26.
118. King MA, Long DT, Brill AR. SPECT volume quantitation: influence of spatial resolution, source size and shape and voxel size. *Med Phys* 1991; 18:1016–1024.
119. Long DT, King MA, Sheehan J. Comparative evaluation of image segmentation methods for volume quantitation in SPECT. *Med Phys* 1992;19:483–489.
120. Long ET, King MA, Penney BC. Two-dimensional versus three-dimensional edge detection as a basis for volume quantitation in SPECT. *Prog Clin Biol Res* 1991;363:457–471.
121. Goris ML, Daspit SG, McLaughlin P, Kriss JP. Interpolative background subtraction. *J Nucl Med* 1976;17:744–747.
122. Glickman S. Determination of organ volume with SPECT. *SPIE Proc* 1987;767:406–410.
123. Hoffman EJ, Huang SC, Phelps ME. Quantitation in positron emission computed tomography. I. Effect of object size. *J Comput Assist Tomogr* 1979;3:299–308.
124. Pretorius PH, van Aswegen AI, Herbst CP, Lotter MG. The effects of different correction techniques on absolute volume determination with SPECT using a threshold edge detection method. *Med Phys* 1991;18:390–393.
125. Mortelmans L, Nuyts J, Van Pamel G, Vander Maegdenbergh V, DeRoo M, Suetens P. A new thresholding method for volume determination by SPECT. *Eur J Nucl Med* 1986;12:284–290.
126. Ballard DH, Brown CM. *Computer Vision*. Englewood Cliffs, NJ: Prentice-Hall, 1982;76–84.
127. Otsu N. A threshold selection method from gray-level histograms. *IEEE Trans Sys Man Cyber* 1979;9:62–66.
128. Tsui BMW, Zhao X, Frey EC, McCartney WH. Quantitative single-photon emission computed tomography: basics and clinical considerations. *Semin Nucl Med* 1994;24:38–65.
129. Moore SC, Kouris K, Cullum I. Collimator design for single-photon emission tomography. *Eur J Nucl Med* 1992;19:138–150.